Modelling the effects of sediment compaction on salt marsh reconstructions of recent sea-level rise

Matthew J. Brain[a1], Antony J. Long[a], Sarah. A Woodroffe[a], David N. Petley[a], David G. Milledge[a] and Andrew C. Parnell[b]

[a] *Department of Geography, Durham University, Science Site, South Road, Durham, DH1 3LE, UK*

[b] *School of Mathematical Sciences (Statistics), University College Dublin, Library Building, Belfield, Dublin 4, Ireland*

Abstract

This paper quantifies the potential influence of sediment compaction on the magnitude of nineteenth and twentieth century sea-level rise, as reconstructed from salt marsh sediments. We firstly develop a database of the physical and compression properties of low energy intertidal and salt marsh sediments. Key compression parameters are controlled by organic content (loss on ignition), though compressibility is modulated by local-scale processes, notably the potential for desiccation of sediments. Using this database and standard geotechnical theory, we use a numerical modelling approach to generate and subsequently 'decompact' a range of idealised intertidal stratigraphies. We find that compression can significantly contribute to reconstructed accelerations in recent sea level, notably in transgressive stratigraphies. The magnitude of this effect can be sufficient to add between 0.1 and 0.4 mm yr^{-1} of local sea-level rise, depending on the thickness of the stratigraphic column. In contrast, records from shallow (< 0.5 m) uniform-lithology stratigraphies, or shallow near-surface salt marsh deposits in regressive successions, experience negligible compaction. Spatial variations in compression could be interpreted as 'sea-level fingerprints' that might, in turn, be wrongly attributed to oceanic or cryospheric processes. However,

[1] Corresponding author. Department of Geography, Durham University, Science Site, South Road, Durham, DH1 3LE, UK. Tel: +44 (0)191 334 3513; Fax: +44 (0)191 334 1801.
Email address: matthew.brain@durham.ac.uk

consideration of existing sea-level records suggests that this is not the case and that compaction cannot be invoked as the sole cause of recent accelerations in sea-level inferred from salt marsh sediments.

Keywords: Compaction; compression; salt marsh; sea-level acceleration.

1. Introduction and aim

Considerable interest is focussed on the possibility of an acceleration in global sea-level rise that has occurred in the last 100 – 200 years. Twentieth century rates of global sea-level rise recorded by tide gauges (1.7 – 1.8 mm yr^{-1}; Bindoff *et al*., 2007; Church and White, 2006; Douglas, 1991) are greater than those obtained from the geological record of Late Holocene sea-level rise (e.g. Shennan and Horton, 2002; Engelhart *et al*., 2009; Gehrels *et al*., 2012). Constraining the magnitude, timing and spatial variability of this acceleration is critical to our understanding of atmosphere-cryosphere-ocean interactions. However, there are few pre-1900 tide gauge records and those that exist are concentrated in NW Europe, limiting their use in resolving this matter (Douglas, 1992; Woodworth *et al*., 2009). An alternative approach is to use the proxy sea-level records contained within salt marsh stratigraphies (Gehrels, 2000; Scott and Medioli, 1978). Consequently, an increase in the rate of sea-level rise in the late nineteenth to early twentieth century has been identified in several sea-level reconstructions derived from salt marshes in the northern (Donnelly *et al*., 2004; Gehrels *et al*., 2005; 2006; Kemp *et al*., 2009; Leorri *et al*., 2008) and southern hemispheres (Gehrels *et al*., 2008; 2012). This phenomenon has been attributed to a combination of natural and anthropogenic influences (cf. Kemp *et al*., 2011; Mann and Jones, 2003).

A critical assumption of the salt marsh approach is that the effects of sediment compaction on these low-energy, organic sedimentary deposits are negligible. Compaction involves a combination of physical and biochemical processes that reduces the vertical thickness of the sediment column (Allen, 2000), distorting stratigraphic sequences (Allen,

1999; Bloom, 1964; Haslett *et al*., 1998; Jelgersma, 1961; Kaye and Barghoorn, 1964). Compaction lowers 'sea-level index points' (SLIs) from their depositional altitudes (Edwards, 2006), introducing a potentially significant error into sea-level reconstructions obtained from salt marshes and associated low energy intertidal stratigraphies (Long *et al*., 2006). Since the effects of compaction are time-dependent, there is a further possibility that surface lowering of a salt marsh could be misinterpreted as a 'real' acceleration in the rate of sea-level rise. Unfortunately, the contribution of compaction to salt marsh-based reconstructions of recent sea level is currently poorly constrained. Our aim is to address this critical issue by quantifying the potential contribution of sediment compression, a key compaction process that describes volumetric changes in response to applied overburden pressures, to the recent acceleration in salt marsh-based sea-level reconstructions.

2. Sediment compaction

Late Holocene stratigraphic studies report rates of compaction that are regional estimates averaged over centennial to millennial timescales and/or obtained from multiple, often thick (5 – 10 m) stratigraphic sections (Horton and Shennan, 2009; Törnqvist *et al.*, 2008). These studies lack sufficient resolution to be applicable to the shallower sections (< 3 m) and shorter timescales (decadal to centennial) typical of recent salt marsh studies. Basal salt marsh peats that directly overlie an incompressible surface can provide a compaction-free sea-level record (Törnqvist *et al*., 2004). However, to date only one (Donnelly *et al*., 2004) of the published high-resolution salt marsh reconstructions of sea level for the last 200 years uses basal peats; the others rely on continuous salt marsh stratigraphies.

Numerical modelling of compaction provides an alternative approach to solely field-based studies (Massey *et al*., 2006; Paul and Barras, 1998; Pizzuto and Schwendt, 1997). However, such models often employ classical soil mechanics theories that may not be suitable in low energy intertidal settings, where unique lithologies form and where the stress

and diagenetic environments are distinct. Indeed, Brain *et al*. (2011) studied the compression behaviour of minerogenic tidal flat and salt marsh sediments and found a difference to that assumed in standard geotechnical compression models because of overconsolidation at the depositional surface, meaning that they have experienced an effective compressive stress greater than that exerted by the existing overburden (Powrie, 2004). Overconsolidated sediments exhibit a reduced compressibility state until the previous maximum value of effective stress experienced by the sediment (the yield stress) is exceeded. Brain *et al.* (2011) explained the observed compression behaviour of these sediments in terms of organic content and the frequency and duration of tidal immersion, which are both controlled by elevation within the intertidal zone, and developed a theoretical framework that describes compression behaviour within NW European low energy intertidal settings. This framework describes variations in compression behaviour with reference to a four-parameter model (Figure 1).

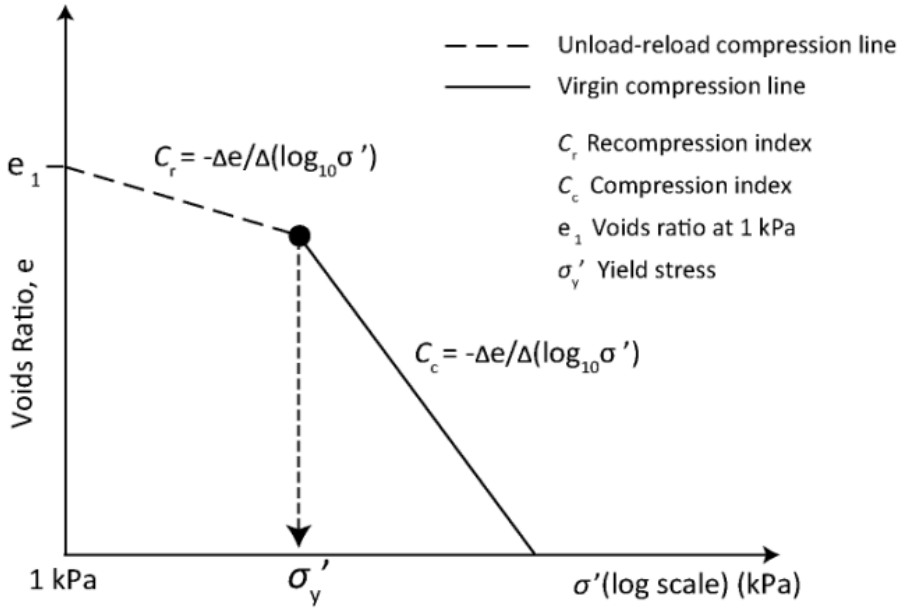

Figure 1 Four-parameter model to describe compression behaviour in low energy intertidal sediments. See text for further description.

3. The compression property database

3.1 Field data collection

We studied three UK field sites that vary in geomorphic setting, hydrographic conditions and eco-sedimentological characteristics: Cowpen Marsh, Roudsea Marsh and Thornham Marsh (Figure 2; see Supplementary Information). At each site, we recorded vegetation assemblages, logged sample lithology and described the physical and geotechnical properties of samples in accordance with Keble Martin (1974) and British Standards Institute (2002).

We collected undisturbed sediment samples (British Standards Institute, 1999) from the upper 0.2 m of the sediment column (i.e. the depositional surface) from each eco-sedimentological zone for laboratory testing. Samples were stored in confined, sealed and cold conditions (*c*. 4˚ C) to prevent disturbance due to stress relief, moisture loss and to limit bacterial processes.

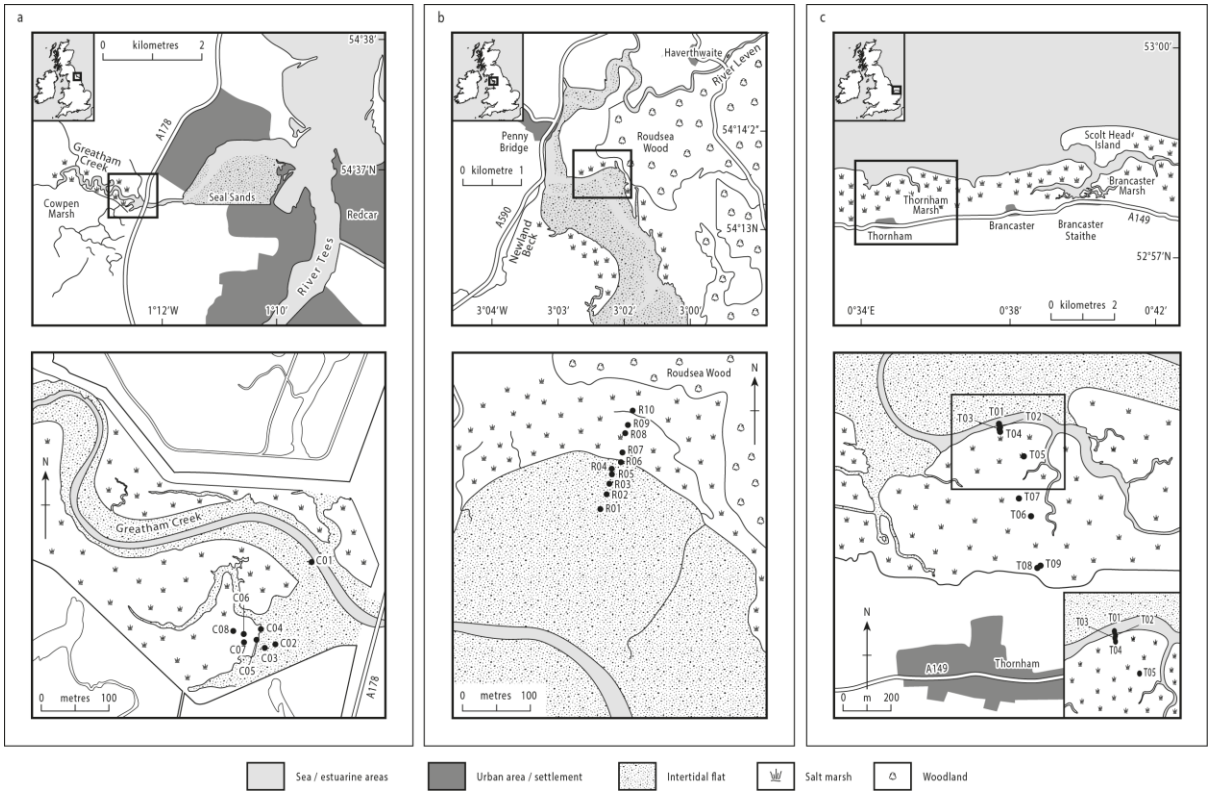

Figure 2 Field site and sampling locations maps for (a) Cowpen Marsh, (b) Roudsea Marsh and (c) Thornham Marsh.

3.2 Laboratory methods

We determined organic content by loss on ignition (LOI; 550˚C for 4 hours) and particle size by laser granulometry (see Brain *et al*., 2011). We determined sediment physical properties (moisture content, specific gravity, bulk density, voids ratio by Height of Solids) in accordance with BS 1377 (British Standards Institute, 1990; Head, 1988). One-dimensional, K_0 (zero lateral strain) compression testing was undertaken using fixed ring, front-loading oedometers in general accordance with BS 1377 (British Standards Institute, 1990; Head, 1988), but with modifications outlined by Brain *et al*. (2011). Each loading stage lasted 24 hours.

3.3 Numerical and analytical techniques

Due to the differences in tidal range between the sites, it is necessary to standardise water levels to allow comparison of elevation data, which we use as a surrogate for the frequency and duration of tidal flooding and subaerial exposure. We have used the Standardised Water Level Index (SWLI) method (Horton and Edwards, 2006) which linearly standardises the height between two tidal levels, Mean High Water of Spring Tides (MHWST, where SWLI = 100) and Mean Low Water of Spring Tides (MLWST, where SWLI = 0). We have estimated the compressive yield stress, σ'_y, using changepoint regression modelling (Carlin *et al*., 1992; Lunn *et al*., 2000; Parnell, 2005).

3.4 Compression behaviour and properties

LOI, initial voids ratio (e_i, the voids ratio at the depositional surface) and compression indices (C_r and C_c) all vary directly with SWLI (Figure 3). e_i, C_r and C_c all covary strongly with LOI, suggesting that organic content exerts a significant control on these compression properties (Figure 4). These relationships occur despite variability in site characteristics (see Supplementary Information).

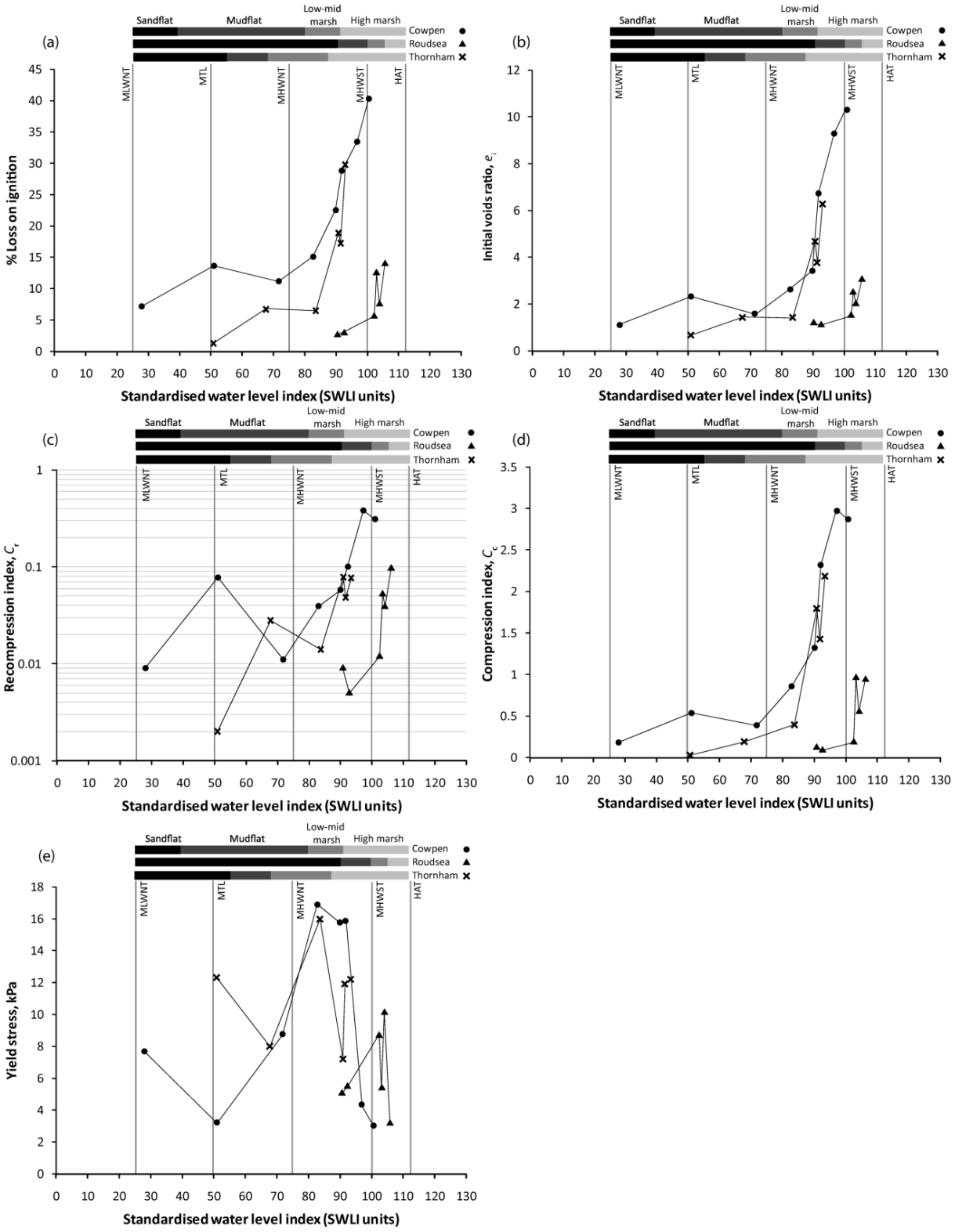

Figure 3 Variations in loss on ignition (a) and compression model parameters (b, c, d, e) with standardised water level index at Cowpen, Roudsea and Thornham Marshes. MLWNT is Mean Low Water Neap Tide level; MTL is Mean Tide Level; MHWNT is Mean High Water Neap Tide Level; MHWST is Mean High Water Spring Tide level; HAT is Highest Astronomical Tide level.

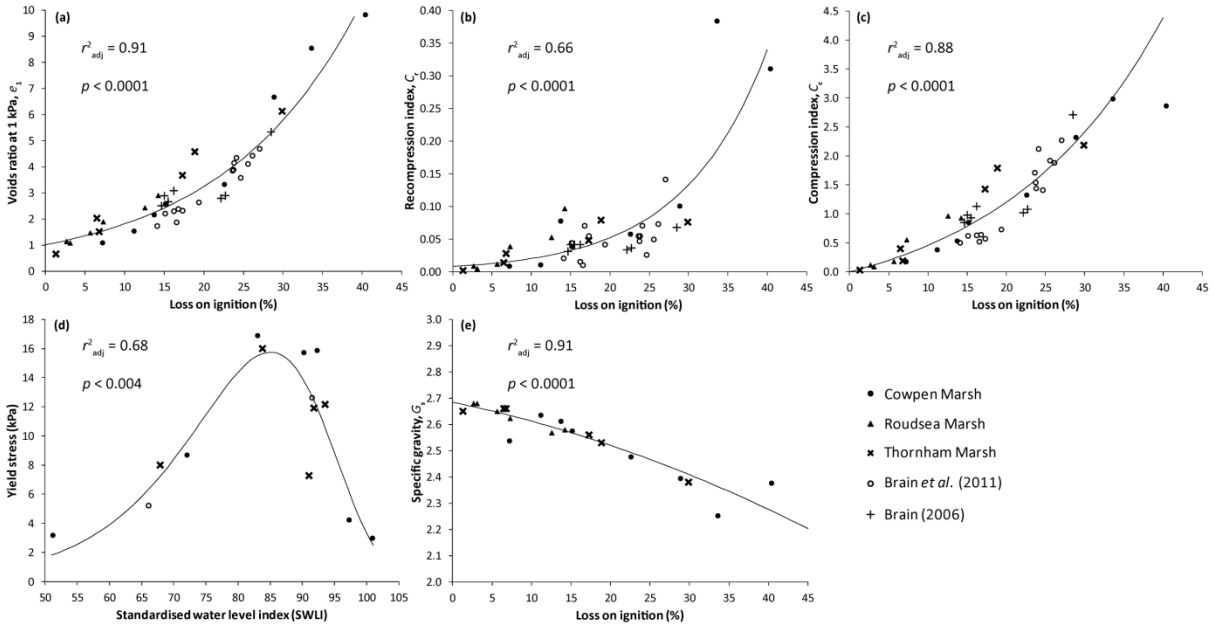

Figure 4 Variations of key compression and physical properties with controlling variables, demonstrating the goodness of fit and statistical significance of predictive regression models. Where available, new data are supplemented with data from previous studies at Cowpen Marsh using contemporary sediments (Brain *et al*., 2011) and near-surface core samples (Brain, 2006). In Figure (d), we use only data from Cowpen Marsh and Thornham Marsh to develop the regression model, which display similar trends. In addition, we do not use samples obtained from sandflat deposits, since these environments are not investigated as part of the modelling element.

Similar trends in yield stress with SWLI were observed at each of the three sites. These trends are characterised by a rise in σ'_y from minima in the sandflat and mudflat samples to peaks in the low and mid marsh zones. From peak values, σ'_y decreases with SWLI to minima in the high marsh (Figure 3). We observed some local variability in absolute values, but not in trends. We attribute reduced values of σ'_y at Roudsea Marsh to the sand-rich nature of the intertidal zone, which prevents high suction stresses from being achieved during groundwater falls and subaerial desiccation.

3.5 Controls on compression behaviour

The relationships between lithology and e_i, C_r and C_c have a sound physical basis. High organic contents reflect the growth of vascular plant species, which create well-aerated, highly porous soil structures (Delaune *et al*., 1994), and hence higher values of e_i. In addition, reduced flow velocities on salt marshes caused by the frictional drag of vegetation (e.g. Leonard and Luther, 1995) create more open microstructures compared to those observed in tidal flat environments, where flow velocities are greater (Burland, 1990). Less dense sediments are more prone to compression than their denser equivalents (Burland, 1990; Price *et al*., 2005; Skempton, 1970). In addition, organic-rich sediments are more prone to compression than their minerogenic equivalents, since organic matter is compressible (Head, 1988). In contrast, sediments with lower values of e_i, C_r and C_c accumulate lower in the intertidal zone (Figure 3) where suspended sediment concentrations are greater during periods of tidal flooding (Shi *et al*., 2000). Hence, denser sediments (lower values of e_i) form here as a result of higher sedimentation rates from a denser suspension (Been and Sills, 1981; Sills, 1998). The absence of vascular plant growth also prevents the formation of organogenic, open microstructures.

We suggest that the yield stresses, σ'_y, recorded in the surface sediments result from two interacting factors. The rising trend in σ'_y that peaks in the low marsh (Figure 3) results from

increasing subaerial desiccation associated with a reduction in flooding frequency and duration with increasing elevation. The post-peak decline in yield stress in the higher marsh, most apparent at Cowpen Marsh but also suggested by the data for Thornham and Roudsea Marshes (Figure 3), likely records the shift from below-ground to above-ground productivity as vegetation assemblages change (de Leeuw and Buth, 1991). Increased above-ground biomass permits the production of decaying mats of vegetation, which increase in thickness with elevation (see Supplementary Information) and reduce the potential for desiccation. Secondly, an increase in organic content reduces the influence of the cohesive component of the sediment in sustaining suction pressures (cf. Hawkins, 1984). Air entry and desaturation are likely to occur at significantly lower suction stresses than in the fine-grained, minerogenic sediments of the mudflat and low marsh zones, thereby limiting the maximum yield stress that can be achieved by desiccation.

3.6 An improved compression framework

Our findings help us to refine the compression framework for intertidal sediments proposed by Brain *et al*. (2011). Importantly, our new dataset confirms that values of near-surface voids ratio (e_1) and compression indices (C_r and C_c) are controlled by organic content (a function of intertidal elevation), regardless of geomorphic setting and eco-sedimentary conditions (Figure 4).

The controls on yield stress vary in response to feedbacks relating to organic content and the proportion of above-ground biomass production (again, both functions of elevation) that reduce the value of yield stress observed in the high marsh. Despite similar trends observed at each of the sites, absolute values of σ'_y and the ways in which they vary are site-specific. Nevertheless, it is possible to fit a statistically significant regression model to the variations in σ'_y with SWLI with sufficient data, as demonstrated in Figure 4(d). Minor extrapolation suggests that the highly organic sediments forming in the high marsh are likely to be only

very lightly overconsolidated, or indeed normally consolidated. Hence, high marsh sediments are the most compressible (high C_r and C_c), but also may not experience a low compressibility phase (low or absent σ'_y). However, the minimum effective stress value replicated in our oedometer tests is *c.* 3 kPa and so we have no direct empirical evidence of fully normally consolidated sediments.

The strength and significance of the relationships in Figure 4 indicate that the first-order, routine decompaction of intertidal sediments may be possible without the need for extensive geotechnical testing (cf. Paul and Barras, 1998; Skempton, 1944). This is potentially an extremely useful tool for sea-level research, since LOI and SWLI values are routinely determined during stratigraphic and basic laboratory investigations. However, the current database would need to be expanded to ensure that the characteristics of the study sites of interest are adequately captured (see Section 6.5)

4. Compression modelling

4.1 Modelled stratigraphic successions

We now generate, and then 'decompact', a series of synthetic stratigraphic successions that vary in thickness and the depositional sequencing of lithologies. We define stratigraphies that broadly reflect the thickness ranges of existing salt marsh records of late Holocene/twentieth century accelerations (Gehrels *et al*., 2005; 2006; 2008; 2012; Kemp *et al*., 2009; Leorri *et al*., 2008). Such stratigraphies range in contemporary thickness from *c.* 0.5 to 3 m. The acceleration is generally recorded at depths < 0.5 m below ground level (m bgl).

The ideal lithostratigraphic succession for reconstructing sea level is an uninterrupted, highly organic marsh deposit that formed close to high tide level, where accumulation is most tightly controlled by sea-level rise (Allen, 1995; 2000; Gehrels *et al*., 2005). Hence, we firstly consider such 'stable' stratigraphies using the most organic materials in our compression

database. Our modelled stable stratigraphies are uniform, displaying no change in lithology other than minor intra-stratum (stochastic) variability.

A number of recent palaeoecological and numerical studies suggest that the recent sea-level acceleration has resulted in 'transgressive' sediment successions caused by the inability of salt marshes to keep pace with sea level (Donnelly and Bertness, 2001; Kirwan and Temmerman, 2009). In this case, lowering of the salt marsh surface relative to sea level results in an increased minerogenic component and an increased sedimentation rate (Allen, 2000; Pethick, 1981). In our modelled transgressive successions, the stratigraphy records a deepening of water depths; higher marsh deposits are overlain by sediments that accumulate lower in the intertidal frame.

We also consider 'regressive' (shallowing-upward) stratigraphies, which are typical of South Pacific areas where mid- to late Holocene sea levels were largely stable (Gehrels *et al*., 2008; 2012). Our modelled regressive stratigraphies record the upwards replacement of tidal flat by salt marsh deposits.

Table 1 provides a summary of modelled stratigraphic successions.

Table 1 Summary of synthetic stratigraphic successions generated and decompacted.

Succession ID	Succession thickness	Stratum 1			Stratum 2			Stratum 3		
		Depth range (m bgl)	**Mean loss on ignition (%)**	**Sedimentation rate (mm yr^{-1})**	**Depth range (m bgl)**	**Mean loss on ignition (%)**	**Sedimentation rate (mm yr^{-1})**	**Depth range (m bgl)**	**Mean loss on ignition (%)**	**Sedimentation rate (mm yr^{-1})**
Stable/uniform successions										
Acceleration occurs at 0.25 m bgl. Depth range relevant to sea level reconstruction: 0.0 – 0.48 m bgl.										
1	0.5 m	0.0 – 0.5	39	2	-	-	-	-	-	-
2	1 m	0.0 – 1.0	39	2	-	-	-	-	-	-
3	2 m	0.0 – 2.0	39	2	-	-	-	-	-	-
4	3 m	0.0 – 3.0	39	2	-	-	-	-	-	-
Transgressive successions										
Acceleration occurs at 0.4 m bgl. Depth range relevant to sea level reconstruction: 0.0 – 0.64 m bgl.										
5	1 m	0.0 – 0.36	35	3.3	0.36 – 0.4	37	3.3	0.4 – 1.0	39	2
6	2 m	0.0 – 0.36	35	3.3	0.36 – 0.4	37	3.3	0.4 – 2.0	39	2
7	3 m	0.0 – 0.36	35	3.3	0.36 – 0.4	37	3.3	0.4 – 3.0	39	2
8	1 m	0.0 – 0.36	33	3.3	0.36 – 0.4	35	3.3	0.4 – 1.0	39	2
9	2 m	0.0 – 0.36	33	3.3	0.36 – 0.4	35	3.3	0.4 – 2.0	39	2
10	3 m	0.0 – 0.36	33	3.3	0.36 – 0.4	35	3.3	0.4 – 3.0	39	2
11	1 m	0.0 – 0.36	30	3.3	0.36 – 0.4	33	3.3	0.4 – 1.0	39	2
12	2 m	0.0 – 0.36	30	3.3	0.36 – 0.4	33	3.3	0.4 – 2.0	39	2
13	3 m	0.0 – 0.36	30	3.3	0.36 – 0.4	33	3.3	0.4 – 3.0	39	2
14	1 m	0.0 – 0.36	27	3.3	0.36 – 0.4	32	3.3	0.4 – 1.0	39	2
15	2 m	0.0 – 0.36	27	3.3	0.36 – 0.4	32	3.3	0.4 – 2.0	39	2
16	3 m	0.0 – 0.36	27	3.3	0.36 – 0.4	32	3.3	0.4 – 3.0	39	2
17	1 m	0.0 – 0.36	24	3.3	0.36 – 0.4	30	3.3	0.4 – 1.0	39	2
18	2 m	0.0 – 0.36	24	3.3	0.36 – 0.4	30	3.3	0.4 – 2.0	39	2
19	3 m	0.0 – 0.36	24	3.3	0.36 – 0.4	30	3.3	0.4 – 3.0	39	2

Succession ID	Succession thickness	Stratum 1			Stratum 2			Stratum 3		
		Depth range (m bgl)	Mean loss on ignition (%)	Sedimentation rate (mm yr^{-1})	Depth range (m bgl)	Mean loss on ignition (%)	Sedimentation rate (mm yr^{-1})	Depth range (m bgl)	Mean loss on ignition (%)	Sedimentation rate (mm yr^{-1})
Regressive successions										
Acceleration occurs at 0.24 m bgl. Depth range relevant to sea level reconstruction: 0.0 – 0.5 m bgl.										
20	1 m	0.0 – 0.4	39	2	0.4 – 0.5	24	2.5	0.5 – 1.0	15	Not specified
21	2 m	0.0 – 0.4	39	2	0.4 – 0.5	24	2.5	0.5 – 1.0	15	Not specified
22	3 m	0.0 – 0.4	39	2	0.4 – 0.5	24	2.5	0.5 – 1.0	15	Not specified

Notes: standard deviation of loss on ignition values in each stratum were low (< 1 % loss on ignition), even in single iterations of the model.

4.2 Sub-model 1: Generation of synthetic stratigraphies

Sub-model 1 generates synthetic stratigraphic successions. It uses a repeat-iteration, stochastic (Monte-Carlo) approach to explore the effects of natural environmental variability and regression model error on overall compression trends. We run the model 1000 times for each stratigraphic succession considered (see Supplementary Information).

There are two model inputs, which we consider deterministically: thickness of the sediment column (z, in m) and palaeomarsh surface elevation (PMSE, defined in terms of a contemporary altitude in m OD). Each artificial stratigraphic succession is split into layers of equal thickness (0.02 m, the approximate height of a typical oedometer sample). In each layer, the calculated *in situ* effective stress state and geotechnical properties are assumed to be constant.

A PMSE for each layer is used to generate LOI values, based on established relationships between elevation and LOI (Brain *et al.*, 2011). PMSEs are selected to generate representative downcore LOI profiles, using Cowpen Marsh as our reference study site (site choice does not affect our conclusions). We use the regression models detailed in Section 3 and illustrated in Figure 4 to generate values of e_1, C_r, C_c and specific gravity, G_s in each layer. We convert the specified PMSE to a SWLI value to calculate the yield stress, σ'_y, for each layer using the regression model in Figure 4(d). Output values from the regression models are selected randomly from statistical error distributions (see Supplementary Information). The standard error of the yield stress regression model results in possible predictions of $\sigma'_y < 3$ kPa. Whilst this may be possible, we have no empirical observations of this (Section 3.6). Given the sensitivity of results to low yield stresses, we specify a minimum yield stress value of 3 kPa in all lithologies to prevent extrapolation beyond observed values.

In situ voids ratio values for each layer are calculated using a conditional regression model, formulated as follows:

$$e = e_1 - C_r(\log_{10}\sigma' - \log_{10}\sigma'_y) \textbf{ if } \log_{10}\sigma' \leq \log_{10}\sigma'_y \quad (1a)$$

$$e = e_1 - C_c(\log_{10}\sigma' - \log_{10}\sigma'_y) \textbf{ if } \log_{10}\sigma' > \log_{10}\sigma'_y \quad (1b)$$

where e is the voids ratio predicted by the model, $e_1$is a constant (the value of voids ratio at 1 kPa, calculated during changepoint regression analysis) and σ' is a value of effective stress at the top of the layer under consideration. The logarithmic functions used to describe voids ratio prevent the use of 0 kPa as the value of effective stress at the depositional surface. Instead, we use a value of 0.01 kPa at the depositional surface, which is the order of magnitude of the minimum effective stresses encountered within our modelling experiments (cf. Brain *et al.*, 2011; Smith, 1985).

Beginning with the uppermost layer at the depositional surface, we calculate bulk density (ρ_d, in g/cm^3) as follows:

$$\rho_d = (G_s + e)/(1 + e) \quad (2)$$

This permits calculation of the saturated unit weight (γ_{sat}, in kN/m^3) of the layer:

$$\gamma_{sat} = \rho_d \cdot g \quad (3)$$

where g is the gravitational constant (9.81 m/s^2). We then calculate the total stress (σ) at the base of the layer:

$$\sigma = \gamma_{sat} \cdot t \quad (4)$$

where t is the thickness of the layer in metres. Assuming hydrostatic conditions, we calculate pore water pressure, u, at the base of the layer:

$$u = \gamma_w \cdot d \tag{5}$$

where γ_w is the unit weight of water (9.81 kN/m^3) and d is depth (m) at the base of the layer below the ground surface. We assume no near-surface unsaturated or capillary saturated zones. Effective stress σ' (kPa) acting at the base of the layer can be calculated from:

$$\sigma' = \sigma - u \tag{6}$$

Using this value of effective stress, we can then calculate e, ρ_d, and γ_{sat} in the underlying layer. Hence, the effective stress acting at the base of any layer, $\sigma'_{(n)}$, can therefore be calculated from:

$$\sigma'_{(n)} = \sigma'_{(n-1)} + \left(\left(\gamma_{sat(n)} \cdot t_{(n)}\right) - u_{(n)}\right) \tag{7}$$

where $\sigma'_{(n-1)}$ is the effective stress as the base of the overlying layer, $\gamma_{sat(n)}$ is the saturated unit weight of the layer, $t_{(n)}$ is the thickness of the layer, $u_{(n)}$ is the pore water pressure at the base of the layer.

For each model run, the outputs of sub-model 1 are entered into sub-model 2.

4.3 Sub-model 2: Decompaction routine

Sub-model 2 is deterministic, but is run 1000 times for each stratigraphic succession considered, each time using a different set of model values generated in sub-model 1. The decompaction routine involves sequentially removing layers of sediment, beginning with the

uppermost layer, to calculate the effective stress profile prior to the deposition of the layer removed. For each layer removed, this involves subtracting the value of effective stress at the base of the layer removed from the values of effective stress in every underlying layer. This provides a new effective stress profile, from which we use the compression model (Figure 1; Equations 1a and 1b) to predict values of voids ratio in each layer under the reduced effective stress conditions. Changes in layer thickness with removal of overlying layers can then be calculated using:

$$\Delta t_{(n)} = \frac{t_{(n)} \cdot (e_p - e_s)}{1 + e_s} \quad (8)$$

where $\Delta t_{(n)}$ is the change in thickness of a layer, $t_{(n)}$ is the *in situ*, compacted thickness of the layer, e_p is the model-derived, decompacted voids ratio of the layer and e_s is the *in situ*, compacted voids ratio.

For each layer removed, the decompaction procedure is completed in every underlying layer. The individual thickness changes in each layer are then summed to calculate the total post-depositional lowering (PDL, m) experienced by the layer immediately below that which has been removed since deposition of overburden sediments. PDL is the height correction that must be added to the *in situ* altitude of an individual SLI to return it to its depositional altitude.

4.4 Sub-model 3: Sea level

To demonstrate the effect of compression on sea-level reconstruction, we use an idealised (non-compacted) sea-level curve that contains a recent acceleration, using the depth profile and layer IDs generated earlier in the modelling procedure (Table 1). We assign a year (AD) and sea level (m MSL) to each layer, specifying a pre-inflection rate of 0.2 mm yr^{-1} (cf. Bindoff *et al*., 2007) and a post-inflection rate of 1.5 mm yr^{-1}. We specify an acceleration in

the rate of sea-level rise at 1880, with immediate transition from pre- to post-inflection rates. To determine the effect of compression, we subtract the mean PDL (m) value for a specific layer from its corresponding sea-level value (m). This subtraction results in a distortion of the sea-level record that represents what would be recorded *in situ*, prior to application of a decompaction correction.

5. Results

5.1 Post-depositional lowering profiles

In all uniform (stable) stratigraphies, the form of the depth-PDL plots is similar, characterised by no PDL at the top and base of the sediment column and a mid-column peak (Figure 5). The magnitude of the mid-column PDL peak becomes greater with increases in initial thickness of the sediment column, rising to a maximum of 0.03 m at 1.5 m depth in the 3 m core. The form of the depth-PDL plot is continuously curved, with no obvious inflection point.

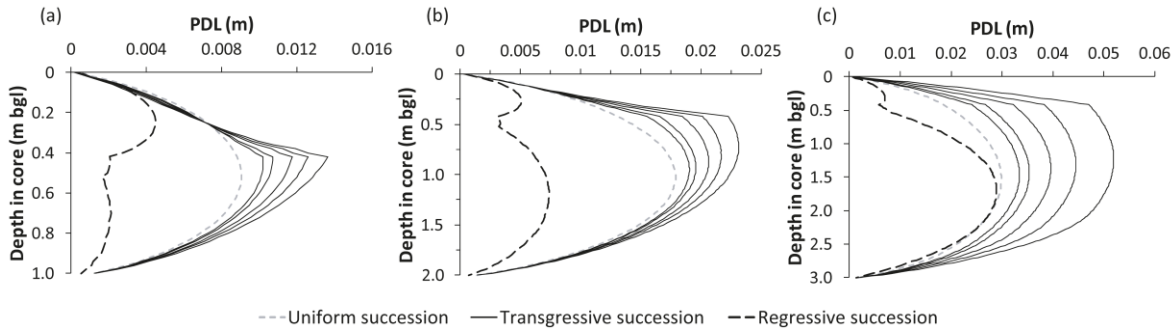

Figure 5 Variations in post-depositional lowering in the modelled cores (1 m, 2 m and 3 m cores only). Note variations in scales of axes. For the transgressive successions, in each graph the mean organic content in the uppermost stratum decreases from left to right: 35 %, 33 %, 30 %, 27 % and 24 %. For clarity, errors on model predictions are not shown.

For the transgressive stratigraphies considered, we vary the mean LOI in the upper transgressive strata (0.0 - 0.4 m) between 24 and 35 % to demonstrate model sensitivity to this parameter. Where the change in lithology resulting from the transgressive overlap is least pronounced, the overall form of the depth-PDL curve is similar to that observed in uniform stratigraphies with peak PDL at the mid-point of the sediment column (Figure 5). However, where more marked changes in lithology occur, maximum PDL occurs higher in the core. Again, PDL is greater in deeper stratigraphies (Figure 5). The maximum value of PDL increases as LOI in the uppermost, transgressive layer decreases (Figure 5). In addition, as the difference in lithology (LOI) becomes more pronounced at the stratigraphic contact, the form of the PDL plot also changes. Rather than a continuously curved depth-PDL profile, the variation in lithology results in an increasingly pronounced inflection in the PDL plot.

In the regressive stratigraphies modelled (Figure 5), the magnitude of PDL again increases in thicker stratigraphies, though the PDL is almost always less than in the modelled uniform and transgressive successions. The form of the depth-PDL plots is markedly different. Each stratigraphic layer has a noticeable peak PDL value that is close to, but not at, the centre of each stratum. In the 1 m core, the peak PDL occurs in the uppermost salt marsh layer. As the sediment column thickens and effective stresses exceed the yield stress in the lower mudflat material, the peak PDL shifts to this lower stratum (Figure 5).

5.2 Influence on reconstructed sea level

The changes predicted in Figure 5 are always less than 0.06 m, but their influence on reconstructed rates of sea-level change is potentially important. Figure 6 shows three examples of the effects of PDL on our synthetic late Holocene/twentieth century sea-level reconstructions. For each we calculated linear rates of sea-level change on the pre- and post-inflection portions of the sea-level curve (Table 2; Figure 7).

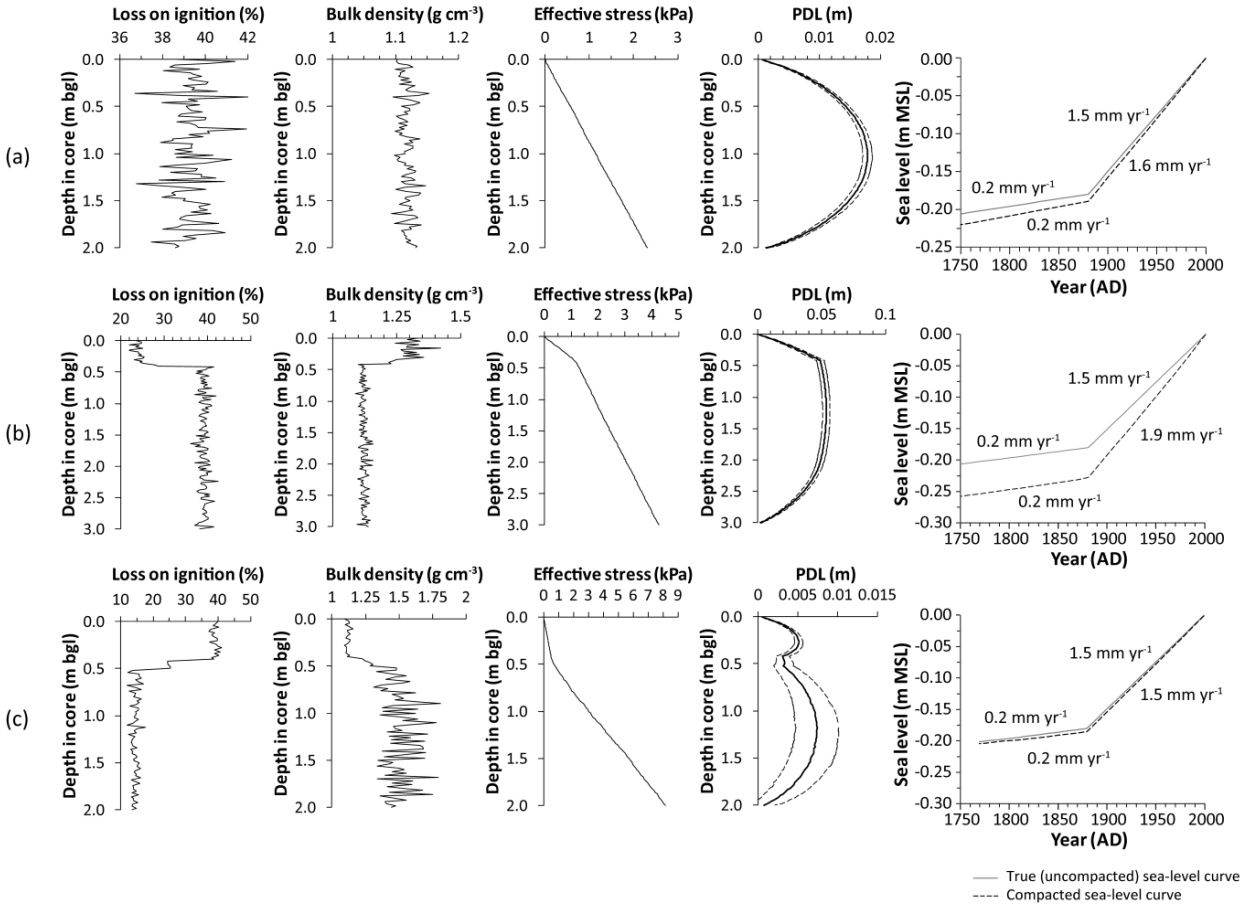

Figure 6 Example model outputs for (a) 2 m uniform succession (Succession ID = 3), (b) 3 m transgressive succession (Succession ID = 16) and (c) 2 m regressive succession (Succession ID = 21). Note differences in scales of axes in each succession. Loss on ignition, bulk density and effective stress profiles are based on single mode iterations to demonstrate similarity with natural cores. Post-depositional lowering (PDL) profiles are based on 1000 model runs and display mean values ± 1 standard deviation for each layer. In the sea level plots, PDL errors are not displayed for clarity, but cluster very closely to the compacted sea level curve.

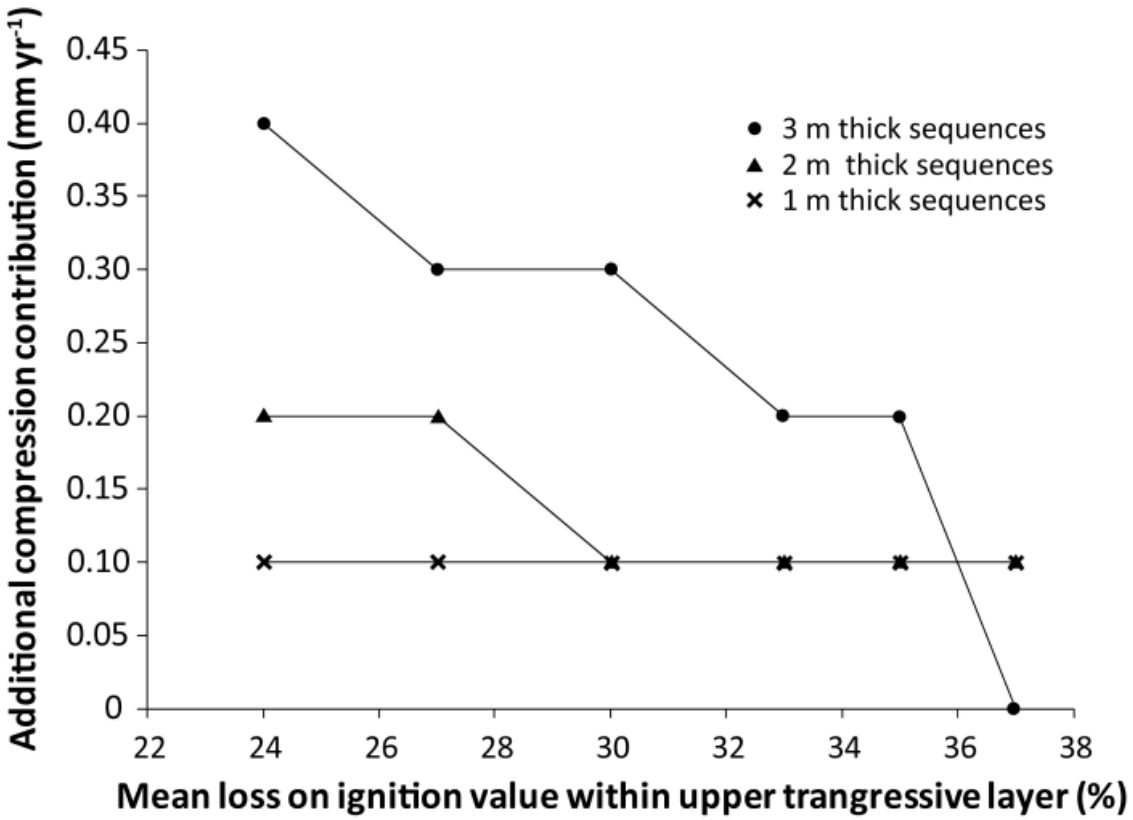

Figure 7 Summary of the modelled total contribution (mm yr^{-1}) of compression to the late Holocene/twentieth century acceleration in sea level for 1 m, 2 m and 3 m thick stratigraphic successions.

Table 2 Summary of the additional contribution of compression/PDL to the magnitude of late Holocene/twentieth century accelerated sea-level rise. Additional compression contributions calculations are based on a modelled 'true' acceleration of 1.3 mm yr^{-1}.

Succession ID	Succession thickness	Mean loss on ignition (%) in Stratum 1	Pre-inflection rate (mm yr^{-1})	Post-inflection rate (mm yr^{-1})	Difference (mm yr^{-1})	Additional compression contribution (mm yr^{-1})
Stable/uniform successions						
1	0.5 m	39	0.2	1.5	1.3	0.0
2	1 m	39	0.2	1.6	1.4	0.1
3	2 m	39	0.2	1.6	1.4	0.1
4	3 m	39	0.3	1.6	1.3	0.0
Transgressive successions						
5	1 m	35	0.2	1.6	1.4	0.1
6	2 m	35	0.2	1.6	1.4	0.1
7	3 m	35	0.2	1.7	1.5	0.2
8	1 m	33	0.2	1.6	1.4	0.1
9	2 m	33	0.2	1.6	1.4	0.1
10	3 m	33	0.2	1.7	1.5	0.2
11	1 m	30	0.2	1.6	1.4	0.1
12	2 m	30	0.2	1.6	1.4	0.1
13	3 m	30	0.2	1.8	1.6	0.3
14	1 m	27	0.2	1.6	1.4	0.1
15	2 m	27	0.2	1.7	1.5	0.2
16	3 m	27	0.2	1.8	1.6	0.3
17	1 m	24	0.2	1.6	1.4	0.1
18	2 m	24	0.2	1.7	1.5	0.2
16	3 m	24	0.2	1.9	1.7	0.4
Regressive successions						
20	1 m	39	0.2	1.5	1.3	0.0
21	2 m	39	0.2	1.5	1.3	0.0
22	3 m	39	0.2	1.5	1.3	0.0

For the uniform stratigraphies considered, the total additional contribution of PDL to accelerated sea-level rise ranges from 0.0 – 0.1 mm yr^{-1}. The greatest overall additional contributions to acceleration are in the uniform 1 m and 2 m cores. However, in the uniform 3 m core, PDL contributes an additional 0.1 mm yr^{-1} to both pre- and post-inflection rates, though the magnitude of the acceleration remains equal to the true sea-level record.

In the modelled transgressive successions, greater contributions of PDL to accelerated sea-level rise occur in thicker deposits (Table 2; Figure 7). The magnitude of the compression contribution in all instances increases as the stratigraphic variation in lithology becomes more pronounced. In 1 m thick stratigraphies, the additional contribution does not exceed 0.1 mm yr^{-1}, regardless of overburden lithology. In 2 m thick stratigraphies, small changes in lithology also result in an additional 0.1 mm yr^{-1}, rising to 0.2 mm yr^{-1} where the transgressive overlap is most marked. In 3 m thick transgressive stratigraphies, our modelling results display a minimum 0.2 mm yr^{-1} additional contribution to the sea-level acceleration. Where changes in organic content (LOI) are most pronounced, the compression contribution rises to 0.4 mm yr^{-1} (Table 2; Figure 7).

In the modelled regressive stratigraphies, the low PDL values result in the lowest compression contribution to accelerated sea level. No major additional contributions are predicted in such stratigraphies.

6. Discussion

6.1 Patterns of post-depositional lowering

Greater PDL occurs in thicker stratigraphies due to higher effective stresses generated by increased overburden thicknesses. As effective stresses in lower layers begin to exceed compressive yield stresses, and transitions from low (C_r) to high (C_c) compressibility behaviour occur, the effect is experienced throughout the sediment column. This is demonstrated by the considerable overall increase in PDL between 2 m and 3 m successions

(Figure 5). The observed mid-column peak in uniform and, to an extent, transgressive successions has previously been reported (Massey *et al.*, 2006; Paul and Barras, 1998; van Asselen *et al.*, 2009) and reflects the optimal combination of loading by overburden sediments and lowering due to compression of underlying material (van Asselen *et al.*, 2009).

The magnitude of PDL in transgressive stratigraphies is considerably greater than in regressive stratigraphies. This results from more compressible sediments being loaded by denser and heavier materials in transgressive successions. In contrast, regressive stratigraphies experience and record the reverse. The greater susceptibility of transgressive stratigraphies to compression relative to their regressive equivalents has been noted previously in both modelling (e.g. Allen, 1999) and field (e.g. Long *et al.*, 2006) studies.

The form of the PDL profiles varies between transgressive and regressive successions. At transgressive overlaps, changes in compression properties associated with LOI result in marked inflections in PDL. The inflection is more pronounced where a change in lithology, and hence relative density and compressibility between strata, is more marked. In regressive successions, PDL peaks occur within individual stratigraphic units and result from the reduced influence of the compression and lowering of underlying sediments and minimised overburden loading.

6.2 Curved and inflected PDL profiles

The continuously curved form of the PDL profiles of uniform stratigraphies is significant for our understanding of the causes of the observed acceleration in recent sea-level reconstructed from salt marsh sediments. Were a uniform stratigraphy to accumulate under a regime of steady sea-level rise (no acceleration), the same continuously curved PDL profile would result. Hence, the effect of PDL would result in a continuously curved sea-level plot. In contrast, the nature of the late Holocene/twentieth century acceleration is not gradual with continuous curvature – it is abrupt and distinct (Donnelly *et al.*, 2004; Gehrels *et al.*, 2005;

2006; 2008; 2012; Kemp *et al*., 2009; Leorri *et al*., 2008). Hence, in such stratigraphies, compression is unlikely to be the sole cause of the observed acceleration due to the distinct differences in the form of the observed and hypothetical sea-level curves.

In transgressive stratigraphies that demonstrate a large change in organic content at stratigraphic contacts, a sharp inflection in the PDL profile will result in a corresponding inflection of the sea-level curve. We note that transgressive stratigraphies reflect a positive sea-level tendency (or an increase in the proximity of marine conditions; Morrison, 1976), rather than being an indication of an acceleration in the rate of sea-level rise. However, the observation and synchroneity of the inflection at multiple salt marsh sites and in tide gauge records suggests that the existence of a transgressive stratigraphic overlap is itself likely to result from an acceleration in sea-level rise. Hence, whilst compression can contribute to the reconstructed and non-corrected magnitude of acceleration, the acceleration is unlikely to solely be an artefact of local-scale compression processes.

6.3 Implications for sea-level investigation and interpretation

The modelled PDL profiles and resultant compacted sea-level curves clearly do not represent all stratigraphies and sea-level histories. Nevertheless, the use of empirical compression datasets, the Monte Carlo approach and the types of stratigraphy modelled allow us to assess the potential contribution of compression to the observed recent acceleration in sea-level rise.

Modelled sea-level reconstructions from transgressive successions that display only subtle variations in lithology are prone to an additional sea-level rise acceleration of 0.1 – 0.2 mm yr^{-1}. This is similar to the average rate at which compaction processes have been estimated to lower SLIs through analysis of basal and intercalated index points (Shennan and Horton, (2002), *c*. 0.2 mm yr^{-1}, and Horton and Shennan (2009), 0.1 – 0.4 mm yr^{-1}. In thicker, more markedly transgressive successions, the additional contribution of compression reached

0.4 mm yr^{-1}, which is closer to estimates obtained from thicker (> 3 m) transgressive stratigraphies of larger UK estuarine systems by Horton and Shennan (2009; 0.6 ± 0.3 mm yr^{-1}) and Edwards (2006; 0.7 – 1.0 mm yr^{-1}). However, comparison of our modelled compaction rates with these longer-term stratigraphic studies is not wholly valid, since compaction rates depend on the timeframe considered (decadal, centennial, millennial), sequence depth, lithology and stratigraphy, and the influence of other processes not considered in our model, such as creep and biodegradation, which may be greater over shorter timescales. For example, Törnqvist *et al*. (2008) reported rates of 5 mm yr^{-1} in the Mississippi Delta in > 5 m sequences over a *c*. 1500 year period.

The lowest model predictions of the additional contribution of compression to accelerated sea-level rise were observed in shallow uniform and regressive stratigraphies (0.0 – 0.1 mm yr^{-1}). Clearly these are the most suitable environments from which to minimise the potential effects of sediment compaction.

Our modelling shows that the compression contribution to an acceleration in sea-level rise is significant and should not be ignored. Compared to a 'true' increase in the rate of sea-level rise of 1.3 mm yr^{-1}, compression-enhanced rates are between 1.4 mm yr^{-1} and 1.7 mm yr^{-1}, equal to between 7 % and 24 % of the observed acceleration. These contributions will be larger where the 'true' sea-level acceleration is smaller. To convert this into real-world impacts, 0.1 – 0.4 mm yr^{-1} of additional sea-level rise is equivalent to the melting of *c*. 40 - 160 km^3 yr^{-1} of land-based ice (40 – 160 Gt yr^{-1} of ice mass loss). The upper values of this range are approaching the equivalent sea-level contribution of ice mass balance loss from the Greenland Ice Sheet in 2006 (260 ± 40 Gt yr^{-1} mass loss, equivalent to 0.6 ± 0.4 mm yr^{-1}; Rignot *et al*., 2011). Hence, accounting for compression is critical for quantifying the magnitude and causes of sea-level rise and in developing predictive models of future sea-level rise.

Our results show that multiple sea-level records obtained from stratigraphies that vary in thickness and lithological sequence ('stable'/uniform, 'transgressive' or 'regressive') may record large apparent variations in historic sea level, despite an identical 'real' sea-level signal. Constraining the compression contribution is therefore important because global spatial variations in the magnitude of accelerated sea-level rise reconstructed from salt marsh records are similar to those predicted by our modelling experiments (cf. Gehrels *et al*., 2012; Kemp *et al*., 2009). Without accounting for compression, such spatial variations could erroneously be attributed to varying cryospheric and/or oceanic forcing, such as the spatial 'fingerprint' of glacier and ice sheet melting resulting from complex interaction of geophysical processes (cf. Mitrovica *et al*., 2001), or latitudinally-variable steric effects (cf. Wake *et al*., 2006).

Gehrels *et al*. (2012) compare salt marsh and tide gauge records of late Holocene/twentieth century sea level and identify a strong latitudinal trend, with faster rates of recent sea-level rise in the southern hemisphere compared with sites further north, leading to the suggestion of a Northern Hemisphere meltwater source for the sea-level acceleration. This spatial variability could, in part, reflect differences in compaction between these sites. The deepest and most strongly transgressive stratigraphies are located on North Atlantic (notably North American) coastlines, whereas the South Pacific salt marshes studied by Gehrels *et al*., (2008, 2012) comprise regressive stratigraphies, with thin high marsh deposits overlying apparently well-consolidated muds. These Southern Hemisphere records are least prone to compression, yet contain the greatest magnitude of sea-level acceleration. Correcting for compaction of the North Atlantic sites would potentially increase the existing differential between these and the South Pacific sites, amplifying any interpreted Northern Hemisphere melt signal.

6.4 Core selection and appraisal of compression

Given the potential problems associated with the use of thick and continuous salt marsh deposits that display variations in lithology throughout the core, the use of compaction-free basal peats provides the best way to limit uncertainty in sea-level reconstructions resulting from sediment compaction (Törnqvist *et al*., 2004). However, where basal peats are not present, or do not adequately cover the timeframe associated with the late nineteenth to early twentieth century sea-level inflection, our results allow us to make clear recommendations for selection of appropriate stratigraphies. Firstly, thinner sediment columns are preferred, since effective stresses are lower and the cumulative effect of compression in underlying layers is reduced. Secondly, abrupt transgressive contacts should be avoided. Linked to this, LOI and bulk density data for stratigraphies used in reconstruction should be routinely presented and discussed.

Comparison of salt marsh reconstructions with tide gauge records is a powerful tool in assessing the trends and errors in each dataset, allowing the salt marsh method to be validated against a compaction-free record (Gehrels *et al*., 2012). Whilst salt marsh records may overlap with corresponding tide gauge records in age-altitude plots, the inherent variability in both datasets should be assessed, perhaps with appropriate statistical tests to consider the significance of any differences that may be explained by sediment compression. If no statistically significant differences in trends are observed, sediment compaction is unlikely to have affected the salt marsh record of sea-level change.

Records of dry or bulk density are commonly used to assess the degree of compaction in cores of salt marsh sediment (e.g. Gehrels *et al*., 2006; Kemp *et al*., 2009). Constant down-core bulk density is thought to indicate that little or no compaction has occurred. However, our study shows that variability in bulk density within a single stratum resulting from the complex interaction of estuarine, biological and subaerial processes may mask any downcore

trend (Figure 8). This is particularly true in short cores that contain overconsolidated sediments, where the range of effective stresses is small and their absolute values are low. Furthermore, an increasing downcore trend in bulk density does not provide any indication of the magnitude and downcore variability in PDL within a core (Figure 8). This is because PDL depends on the cumulative effect of compression in underlying layers and overburden loading, rather than being solely a function of the effective stress state and material properties within a specific layer. Hence, dry or bulk density data provide only a limited insight into potential compaction effects and should not be used to justify 'no compaction' in late Holocene sea-level studies without independent verification.

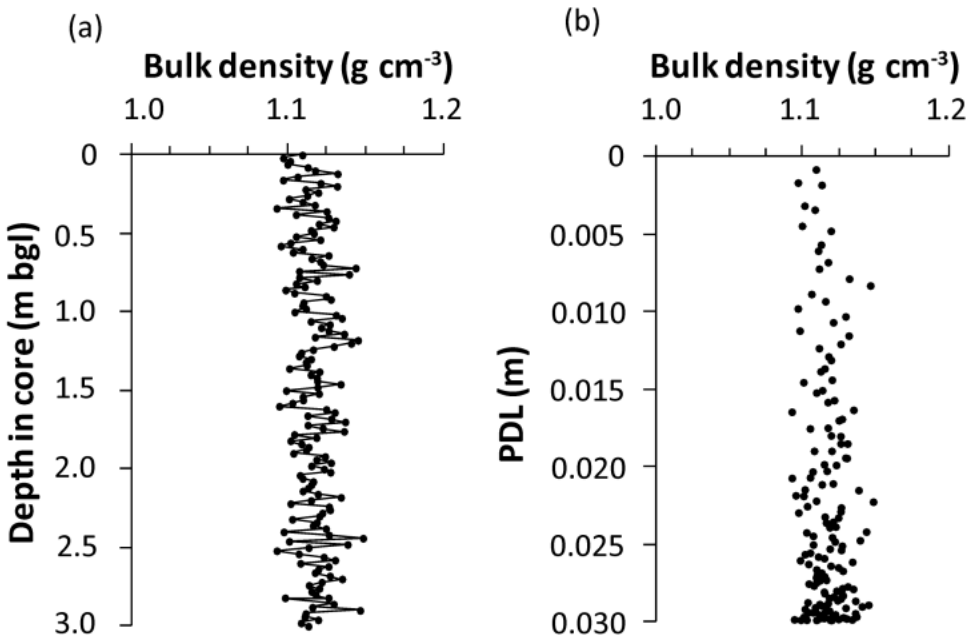

Figure 8 (a) Modelled downcore bulk density profile for a 3 m uniform core (mean loss on ignition = 39 %). (b) Relationship between modelled bulk density and post-depositional lowering for the same modelled core. These data are for a single model iteration to demonstrate variability in predicted values, as would be observed in real-world cores.

6.5 Future research

Our database is based on primarily minerogenic materials typical of UK and similar NW European salt marshes. Voids ratio and compression index values of the most organic materials in our database are similar to those observed in some amorphous and fibrous freshwater peats (cf. Barden, 1969). However, this similarity is only at the lower end of observed values summarised by Hobbs (1986), who reports maximum values of C_c of 10 – 12 and e_i of *c*. 24 - 26. Should more organic salt marsh deposits demonstrate such compressibility, resultant sea-level curves may be affected to a greater degree. However, compressibility is just one control on PDL. Greater voids ratios (lower bulk densities) result in reduced unit weights and, so, effective stresses within intertidal stratigraphies. Our study shows a strong inverse relationship between bulk density and compressibility. Hence, the loading potential of highly compressible organic materials is likely to be considerably smaller and so the effect of greater compressibility may be offset by the generation of lower effective stresses within a stratigraphic succession. Given the more organic-rich nature of North American salt marshes, and given their importance to current discussions regarding sea-level accelerations, it is important that new contemporary data are collected from these marshes to widen our model application.

A second area of future research is to improve our understanding of the role of processes other than overburden loading that can cause compaction, notably biodegradation and creep. These processes are currently poorly understood in salt marsh deposits, though their importance has been shown to be significant in freshwater peats (Hobbs, 1986) and delta environments (van Asselen *et al*., 2011).

Finally, the very low stress (< 3 kPa) compression behaviour of salt marsh deposits represents considerable uncertainty. The mean value of C_c:C_r in our database is 7.31 (standard deviation = 4.42) – i.e. following exceedance of the compressive yield stress,

sediments are 7.31 ± 4.42 times more compressible. Hence, if yield stress values < 3 kPa exist, the high compressibility phase will be active in shorter stratigraphic columns, resulting in greater PDL at shallow depths. However, it is possible that such low values of yield stress may not exist because the zero lateral strain (K_0) compressive stress path is anisotropic and requires internal shear deformation (Addis and Jones, 1986). It is therefore possible that the tensile and shear strength of root material (van Eerdt, 1985; Gabet, 1998) is sufficiently high to prevent internal shear at low stresses and so extremely low yield stresses may be unlikely. Nevertheless, constraining low stress behaviour is an important aim for future research.

7. Conclusions

We have explored the contribution of sediment compression, a key compaction process, to the magnitude of recent accelerated sea-level rise reconstructed from salt marsh sediments. Our conclusions are:

1. Organic content exerts a key control on the structure, density and compressibility of intertidal sediments. We observe statistically significant relationships between LOI and initial voids ratio and compression indices. These relationships occur regardless of local site conditions, such as variations in geomorphic and hydrographic setting, and ecological and sedimentological character. In contrast, the compressive yield stress displays a more complex relationship with a range of site-specific factors relating to both tidal setting, such as flooding frequency and duration, and eco-sedimentary conditions, such as the presence or absence of surface biomass. Yield stress demonstrates greater dependence on local conditions, but a statistically significant predictive relationship can be defined on a site-by-site basis.
2. Identification of the key controls on compression enables the generation of synthetic stratigraphic successions. We subsequently decompact these successions to assess the effects of sediment column thickness and stratigraphic context (‘stable’/uniform

'transgressive' and 'regressive' stratigraphies) on the magnitude of the late Holocene/twentieth century sea-level acceleration reconstructed from salt marsh sediments. Our results show that compression can contribute to, but is unlikely to be the sole cause of, the observed sea-level acceleration.

3. Based on our results, errors associated with compression can largely be avoided by selecting short (< 1 m) uniform successions, or from thin salt marsh deposits that overlie low compressibility tidal flat deposits. Thicker (2 – 3 m) sediment columns that display a pronounced 'transgressive' overlap at the time of the acceleration can contribute an additional component of 0.1- 0.4 mm $yr^{-1}$of sea-level rise.
4. To draw firm conclusions about the magnitude of the effect of compaction in highly organic sediments (>50% LOI) requires collection of new data from organic-rich environments and improved understanding of other compaction processes, including creep and biodegradation.

Acknowledgements

MJB gratefully acknowledges financial support from the Durham University Department of Geography Research Development Fund. We thank Natural England, SABIC Petrochemicals, INEOS/ChlorVinyls and Stephen Bett for permitting access to field sites. Alison Clark, Chris Longley and Neil Tunstall assisted with laboratory work. Samantha Waugh processed GPS data. Figure 2 was drawn by Chris Orton. This paper benefited from discussions with Roland Gehrels, Patrick Kiden and Ben Horton, although the views expressed here remain those of the authors. We thank Torbjörn Törnqvist and an anonymous reviewer for their constructive comments. This paper is a contribution to IGCP 588 'Preparing for Coastal Change' and the PALSEA PAGES/IMAGES/WUN working group: http://eis.bris.ac.uk/~glyms/working_group.html

References

Addis, M.A. and Jones, M.E., 1986. The application of stress path and critical state analysis to sediment deformation. Journal of Structural Geology, 8 (5), 575 – 580.

Allen, J.R.L., 1995. Salt-marsh growth and fluctuating sea level: Implications of a simulation model for Holocene coastal stratigraphy and peat-based sea-level curves. Sedimentary Geology, 100, 21 - 45.

Allen, J.R.L., 1999. Geological impacts on coastal wetland landscapes: Some general effects of sediment autocompaction in the Holocene of northwest Europe. Holocene, 9(1), 1-12.

Allen, J.R.L., 2000. Morphodynamics of Holocene salt marshes: A review sketch from the Atlantic and Southern North Sea coasts of Europe. Quaternary Science Reviews, 19(12), 1155-1231.

Barden, L., 1969. Time-dependent deformation of normally consolidated clays and peats. Journal of the Soil Mechanics and Foundations Division, 95 (1), 1-32.

Been, K. and Sills, G.C., 1981. Self-weight consolidation of soft soils: an experimental and theoretical study. Géotechnique, 31(4), 519-535.

Bindoff, N.L., Willebrand, J., Artale, V., Cazenave, A., Gregory, J., Gulev, S., Hanawa, K., LeQuéré, C., Levitus, S., Nojiri, Y., Shum, C.K., Talley, L.D., Unnikrishnan, A., 2007. Observations: oceanic climate change and sea level. In: Solomon, S., Qin, D., Manning, M., Chen, Z., Marquis, M., Averyt, K.B., Tignor, M., Miller, H.L. (Eds.), Climate Change 2007: The Physical Science Basis: Contribution of Working Group I to the Fourth Assessment Report of the Intergovernmental Panel on Climate Change. Cambridge University Press, Cambridge, United Kingdom and New York, NY, USA, 385–432.

Bloom, A.L., 1964. Peat accumulation and compaction in a Connecticut salt marsh. Journal of Sedimentary Petrology, 34, 599-603.

Brain, M.J., 2006. Autocompaction of Mineralogenic Intertidal Sediments. Unpublished PhD Thesis, Durham University, Durham, UK.

Brain, M.J., Long, A.J., Petley, D.N., Horton, B.P. and Allison, R.J., 2011. Compression behaviour of minerogenic low energy intertidal sediments. Sedimentary Geology, 233, 28–41. doi:10.1016/j.sedgeo.2010.10.005

British Standards Institute, 1990. BS 1377 Methods of test for soils for civil engineering purposes. British Standards Institute, Milton Keynes.

British Standards Institute, 1999. BS 5930 Code of Practice for Site Investigations. British Standards Institute, London.

British Standards Institute, 2002. BS EN ISO 14688-1:2002: Eurocode 7- Geotechnincal investigation and testing –identification and classification of soils – Part 1: indentification and description. British Standards Institute, London.

Burland, J.B., 1990. On the compressibility and shear strength of natural clays. Géotechnique, 40(3), 329-378.

Carlin, B.P., Gelfand, A.E. and Smith, A.F.M., 1992. Hierarchical Bayesian analysis of changepoint problems. Applied Statistics, 41, 389-405.

Church, J.A. and White, N.J., 2006. A 20th century acceleration in global sea-level rise. Geophysical Research Letters, 33, L01602, doi:10.1029/2005GL024826.

Delaune, R.D., Nyman, J.A. and Patrick J, W.H., 1994. Peat collapse, ponding and wetland loss in a rapidly submerging coastal marsh. Journal of Coastal Research, 10(4), 1021-1030.

de Leeuw, J. and Buth, G.J., 1991. Spatial and temporal variation in peak standing crop of European tidal marshes. In: Elliott, M.and Doody,J.P. (eds.), Estuaries and Coasts: Spatial and Temporal Intercomparisons. Olsen and Olsen, Fredensborg, pp. 133 - 137.

Douglas, B.C., 1991. Global sea level rise. Journal of Geophysical Research, 96, 6981–6992. doi: 10.1029/91JC00064.

Douglas, B.C., 1992. Global sea level acceleration. Journal of Geophysical Research, 97, 12699 – 12712. doi: 10.1029/92JC01133.

Donnelly, J.P. and Bertness, M.D., 2001. Rapid shoreward encroachment of salt marsh cordgrass in response to accelerated sea-level rise. Proceedings of the National Academy of Sciences, 98, 14218-14223.

Donnelly, J.P., Cleary, P., Newby, P. and Ettinger, R., 2004. Coupling instrumental and geological records of sea-level change: Evidence from southern New England of an increase in the rate of sea-level rise in the late 19th century. Geophysical Research Letters, 31(5), L05203 1-4.

Edwards, R.J., 2006. Mid- to late-Holocene relative sea-level change in southwest Britain and the influence of sediment compaction. The Holocene, 16(4), 575-587.

Engelhart, S.E., Horton, B.P., Douglas, B.C., Peltier, W.R. and Törnqvist, T.E., 2009. Spatial variability of late Holocene and 20th century sea-level rise along the Atlantic coast of the United States. Geology, 37 (12), 1115-1118. doi: 10.1130/G30360A.1

Gabet, E.J., 1998. Lateral migration and bank erosion in a saltmarsh tidal channel in San Francisco Bay, California. Estuaries, 21,745 - 753.

Gehrels, W.R., 2000. Using foraminiferal transfer functions to produce high-resolution sea-level records from salt-marsh deposits, Maine, USA. The Holocene, 10, 367-376.

Gehrels, W.R., Kirby, J.R., Prokoph, A., Newnham, R.M., Achterberg, E.P., Evans, H., Black, S. and Scott, D.B., 2005. Onset of rapid sea-level rise in the western Atlantic Ocean. Quaternary Science Reviews, 24, 2083-2100.

Gehrels, W.R., Marshall, W.A., Gehrels, M.J., Larsen, G., Kirby, J.R., Eiriksson, J., Heinemeier, J. and Shimmield, T., 2006. Rapid sea-level rise in the North Atlantic Ocean since the first half of the 19th century. The Holocene 16, 948-964.

Gehrels, W.R., Hayward, B.W., Newnham, R.M. and Southall, K.E., 2008. A 20th century sea-level acceleration in New Zealand. Geophysical Research Letters, 35, L02717, doi: 10.1029/2007GL032632.

Gehrels, W.R., Callard, S.L., Moss, P.T., Marshall, W.A., Hunter, J., Milton, J.A. and Garnett, M.H., 2012. High rates of sea-level rise in the Southwest Pacific from the start of the 20th century. Earth and Planetary Science Letters, 315 – 316, 94 – 102. doi:10.1016/j.epsl.2011.08.046

Haslett, S.K., Davies, P., Curr, R.H.F., Davies, C.F.C., Kennington, K., King, C.P. and Margetts, A.J., 1998. Evaluating late-Holocene relative sea-level change in the Somerset Levels, southwest Britain. The Holocene, 8, 197-207.

Hawkins, A.B., 1984. Depositional characteristics of estuarine alluvium: some engineering implications. Quarterly Journal of Engineering Geology, 17, 219-324.

Head, K.H., 1988. Manual of Soil Laboratory Testing: Permeability, Shear Strength and Compressibility Tests. Pentech Press, London/Plymouth.

Hobbs, N.B., 1986. Mire morphology and the properties and behaviour of some British and foreign peats. Quarterly Journal of Engineering Geology, 19, 7-80.

Horton, B.P. and Edwards, R.J., 2006. Quantifying Holocene sea-level change using intertidal foraminifera: lessons from the British Isles. Journal of Foraminiferal Research, Special Publication 40.

Horton, B.P. and Shennan, I., 2009. Compaction of Holocene strata and the implications for relative sea-level change on the east coast of England. Geology, 37, 1083 - 1086.

Jelgersma, S., 1961. Holocene Sea Level changes in the Netherlands. Van Aelst, Maastricht.
Kaye, C.A. and Barghoorn, E.S., 1964. Quaternary sea-level change and crustal rise at Boston, Massachussetts, with notes on the autocompaction of peat. Geological Society of American Bulletin, 75, 63-80.

Keble Martin, W., 1974. The Concise British Flora in Colour. Ebury Press, London.

Kemp, A.C., Horton, B.P., Culver, S.J., Corbett, D.R., van de Plassche, O., Gehrels, W.R. and Douglas, B.C., 2009. The timing and magnitude of recent accelerated sea-level rise (North Carolina, USA). Geology, 37, 1035-1038. doi: 10.1130/G30352A.1

Kemp, A.C., Horton, B.P., Donnelly, J.P., Mann, M.E., Vermeer, M. and Rahmstorf, S., 2011. Climate related sea-level variations over the past two millennia. Proceedings of the National Academy of Sciences, 108, 11017-11022.

Kirwan, M and Temmerman, S., 2009. Coastal marsh response to historical and future sea-level acceleration. Quaternary Science Reviews**,** 28, 1801-1808, doi:10.1016/j.quascirev.2009.02.022

Leorri, E., Horton, B.P. and Cearetta, A. 2008. Development of a foraminifera-based transfer function in the Basque marshes, N. Spain: implications for sea-level studies in the Bay of Biscay. *Marine Geology*, 251, 60-74. doi:10.1016/j.margeo.2008.02.005

Leonard, L. and Luther, M., 1995. Flow hydrodynamics in tidal marsh canopies. Limnology and Oceanography, 40, 1474-1484.

Long, A.J., Waller, M.P. and Stupples, P., 2006. Driving mechanisms of coastal change: Peat compaction and the destruction of late Holocene coastal wetlands. Marine Geology, 225, 63 – 84.

Lunn, D.J., Thomas, A., Best, N., and Spiegelhalter, D., 2000. WinBUGS -- a Bayesian modelling framework: concepts, structure, and extensibility. Statistics and Computing, 10, 325-337.

Mann, M. E., and Jones, P.D., 2003. Global surface temperatures over the past two millennia. Geophysical Research Letters, 30, 1820, doi:10.1029/2003GL017814.

Massey, A.C., Paul, M.A., Gehrels, W.R. and Charman, D.J., 2006. Autocompaction in Holocene coastal back-barrier sediments from south Devon, southwest England, UK. Marine Geology, 226, 225-241.

Mitrovica, J.X., Tamisiea, M.E., Davis, J.L., and Milne, G.A., 2001. Recent mass balance of polar ice sheets inferred from patterns of global sea-level change. Nature, 409, 1026–1029. doi: 10.1038/35059054

Morrison, I.A., 1976. Comparative stratigraphy and radiocarbon chronology of Holocene marine changes on the Western Seaboard of Europe. In: Davidson, D.A. and Shackley, M.L. (eds), Geoarchaeology: Earth Science and the Past. Duckworth, London.

Paul, M.A. and Barras, B.F., 1998. A geotechnical correction for post-depositional sediment compression: examples from the Forth Valley, Scotland. Journal of Quaternary Science, 13(2), 171-176.

Parnell, A.C., 2005. The statistical analysis of former sea level. Unpublished PhD Thesis, University of Sheffield, Sheffield, UK.

Pethick, J.S., 1981. Long-term accretion rates on tidal salt marshes. Journal of Sedimentary Research, 51, 571-577.

Pizzuto, J.E. and Schwendt, A.E., 1997. Mathematical modeling of autocompaction of a Holocene transgressive valley-fill deposit, Wolfe Glade, Delaware. Geology, 25(1), 57-60.

Powrie, W., 2004. Soil Mechanics: Concepts and Applications. Spon Press/Taylor and Francis Group, London and New York.

Price, J.S., Cagampan, J. and Kellner, E., 2005. Assessment of peat compressibility: is there an easy way? Hydrological Processes, 19, 3469 – 3475. doi: 10.1002/hyp.6068

Rignot, E., Velicogna, I., van den Broeke, M.R., Monaghan, A., and Lenaerts, J., 2011. Acceleration of the contribution of the Greenland and Antarctic ice sheets to sea level rise. Geophysical Research Letters, 38, L05503-L05508. doi 10.1029/2011GL046583

Scott, D.B. and Medioli, F.S., 1978. Vertical zonations of marsh foraminifera as accurate indicators of former sea-levels. Nature, 272, 258-531.

Shennan, I. and Horton, B., 2002. Holocene land- and sea-level changes in Great Britain. Journal of Quaternary Science, 17(5-6), 511-526.

Shi, Z., Hamilton, L.J. and Wolanski, E., 2000. Near-bed currents and suspended sediment transport in saltmarsh canopies. Journal of Coastal Research, 16, 909 – 914.

Sills, G., 1998. Development of structure in sedimenting soils. Philosophical Transactions of the Royal Society of London, 356, 2515-2534.

Skempton, A.W., 1944. Notes on the compressibility of clays. Quarterly Journal of the Geological Society of London, 100, 119-135.

Skempton, A.W., 1970. The consolidation of clays by gravitational compaction. Quarterly Journal of the Geological Society of London, 125, 373-411.

Smith, M.V., 1985. The compressibility of sediments and its importance on Flandrian Fenland deposits. Boreas, 14 (1), 1-18.

Törnqvist, T.E., de Jong, A.F.M., Kurnik, C.W., Gonzalez, J.L., Newsom, L.A. and van der Borg, K., 2004. Deciphering Holocene sea-level history on the U.S. Gulf Coast: A high-resolution record from the Mississippi Delta. Bulletin of the Geological Society of America, 116(7-8): 1026-1039.

Törnqvist, T.E., Wallace, D.J., Storms, J.E.A., Wallinga, J., Van Dam, R.L., Blaauw, M., Derksen, M.S., Klerks, C.J.W., Meijneken, C. and Snijders, E.M.A., 2008. Mississippi Delta subsidence primarily caused by compaction of Holocene strata. *Nature Geoscience*, 1, 173-176. doi:10.1038/ngeo129

van Asselen¸ S., Stouthamer, E. and van Asch, Th.W.J., 2009. Effects of peat compaction on delta evolution: A review on processes, responses, measuring and modelling. Earth Science Reviews, 92, 35 – 51.

van Asselen, S., Karssenberg, D. and Stouthamer, E., 2011. Contribution of peat compaction to relative sea-level rise within Holocene deltas, Geophysical Research Letters, 38, L24401, doi:10.1029/2011GL049835.

van Eerdt, M.M., 1985. Salt marsh cliff stability in the Oosterschelde. Earth Surface Processes and Landforms, 10, 95-106.

Wake, L., Milne, G. and Leuliette, E., 2006. 20th century sea-level change along the eastern US: Unraveling the contributions from steric changes, Greenland ice sheet mass balance and late Pleistocene glacial loading. Earth and Planetary Science Letters, 250, 572 – 580.

Woodworth, P.L., White, N.J., Jevrejeva, S., Holgate, S.J., Church, J.A., and Gehrels, W.R., 2009. Review: Evidence for the accelerations of sea level on multi-decade and century timescales: International Journal of Climatology, 29, 777– 789, doi: 10.1002/joc.1771

Brain, M.J., Long, A.J., Woodroffe, S.A., Petley, D.N., Milledge, D.G. and Parnell, A.C.

Modelling the effects of sediment compaction on salt marsh reconstructions of recent sea-level rise

Supplementary Information

1. Detailed study site descriptions

We undertook field work at Cowpen, Roudsea and Thornham Marshes in April, June and July 2010, respectively.

Cowpen Marsh is located in the Tees Estuary on the northeast coast of England, approximately 5 km west of Redcar (Figure 2a). The site has a spring tidal range of 4.6 m (tidal data for River Tees Entrance, obtained from Admiralty Tide Tables, 2005). Roudsea Marsh is located on the northwest coast of England, approximately 3 km southwest of Haverthwaite (Figure 2b). Intertidal sandflats fringe the River Leven. Roudsea Marsh has a spring tidal range of 8.4 m (tidal data for Morecambe Bay, obtained from Admiralty Tide Tables, 2005). Thornham Marsh is located on the North Norfolk coast of England, and comprises an open-coast, back-barrier marsh (Allen, 2000). Thornham Marsh has a spring tidal range of 6.4 m (tidal data for Hunstanton, obtained from Admiralty Tide Tables, 2005).

Eco-sedimentary zones at each site are listed Table S1 and displayed in Figure 3. Sandy deposits occupied the lowermost section of the intertidal zone at each of our three study sites. These graded upwards into mudflat and, subsequently, salt marsh deposits. Low, mid and high marsh macrophyte communities are present at each site. Pioneer marsh assemblages were observed at Cowpen Marsh and Roudsea Marsh. *Puccinellia maritima* and *Salicornia europea* dominate the low marsh species assemblages. Mid and high marsh vegetation assemblages are more unique at each site. At Cowpen Marsh, the mid and high marsh zones are characterised by the dominance of *Sueda maritima*, *Aster tripolium*, *Limonium vulgare*, *Elymus pycnanthus* and *Festuca* spp. In contrast, the mid and high marsh zones at Roudsea Marsh are dominated by *Juncus maritima* and *Phragmites* spp. respectively, whereas

Puccinellia maritima, *Halimione portulacoides* and *Juncus* spp are the principal mid and high marsh plant types at Thornham Marsh.

The elevation (SWLI) ranges occupied by different eco-sedimentary zones varied (Table S1; Figure 3). Mudflat environments occupy the largest SWLI range (*c.* 38 – 81) at Cowpen Marsh, extending below Mean Tide Level (MTL). Low and mid marsh environments at Cowpen Marsh are located above MHWNT within a SWLI range of *c.* 86 to 90, with high marsh present above 93. High marsh is present above similar elevations at Thornham Marsh (SWLI of 91), though the low and mid marsh zones extend to elevations below MHWNT. In marked contrast, the sandflat deposits at Roudsea Marsh are present to standardised elevations (SWLI of 92) that are comparable to the transition to high marsh at Cowpen and Thornham Marshes. Low and mid marsh assemblages are only present above MHWST at Roudsea Marsh, with the transition to high marsh occurring at a SWLI value of 105, between MHWST and Highest Astronomical Tide Level (HAT). Salt marsh deposits at Roudsea Marsh are located at considerably greater standardised elevations within the tidal frame.

Similar trends in sedimentological variables (LOI; sand, silt and clay fractions) are observed at all sites (Table S1; Figure 3; Figure S1). These trends reflect site-specific eco-sedimentary and vegetation zones and their variations in standardised elevational range described above. All sites display an increase in organic content with increased elevation. LOI increases rapidly at the transition from mid- to high marsh. All sites also display a fining of the grain size distribution with increased elevation. Sand contents drop to their lowest values in the mid and high marshes, whilst the relative abundance of silt and clay increase with elevation. Silt contents tend to reach their maximum values in the low and mid marshes, but the proportion of clay falls as elevation increases.

Cowpen Marsh has the highest organic content of the three sites. The clastic component at Cowpen Marsh is dominated by the silt fraction. The lithology of Thornham Marsh is

similar, but the non-vegetated mudflat and sandy deposits are coarser. Roudsea Marsh has a lower organic content and is less clay-rich and more sand-rich sediment in the salt marsh zones.

The differences in the range of standardised elevations (SWLI values) occupied by different eco-sedimentary zones, particularly at Roudsea Marsh, reflect variable tidal range and exposure to wave energy, as controlled by local climate and wave fetch (Gray, 1972), which in turn are partly controlled by geomorphic setting and near-offshore bathymetry (Carniello *et al*., 2011). The regional sediment source is also likely to contribute to the nature of the sediments and their elevational distribution at each site. This is particularly important at Roudsea Marsh, where sediment supply is dominated by the glacial sand deposits of Morecambe Bay. This explains the presence of the widespread fringing sandflats, which are prone to both wave and aeolian erosive forces during times of tidal immersion and emersion respectively. Wind-blown sand layers can cover newly-established vegetation during deposition (Gray, 1972). Pioneer zones and established salt marshes are therefore restricted to the upper intertidal zone (SWLI > 90) at this site, where reduced energy conditions permit the accumulation of silt (Figure S1). In contrast, lower energy conditions and generally finer deposits at Cowpen Marsh and Thornham Marsh reflect their protected settings.

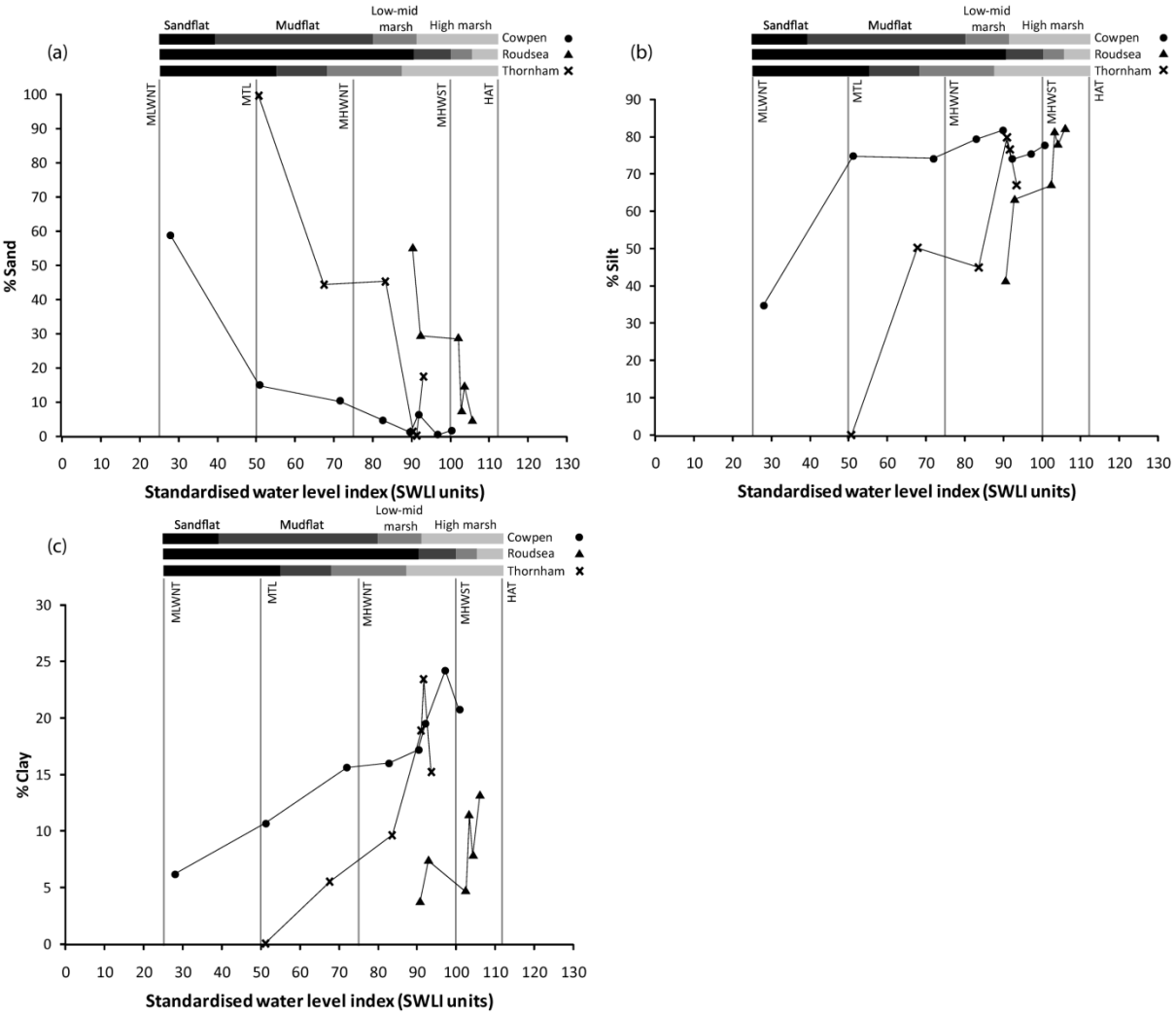

Figure S1 Variations in sand (a), silt (b) and clay (c) content at Cowpen, Roudsea and Thornham Marshes. MLWNT is Mean Low Water Neap Tide level; MTL is Mean Tide Level; MHWNT is Mean High Water Neap Tide Level; MHWST is Mean High Water Spring Tide level; HAT is Highest Astronomical Tide level.

Table S1 Altitudinal/elevational ranges of eco-sedimentary zones and associated vegetation species assemblages at each field site. Altitudinal/elevational ranges are based on single-point measurements and so are approximate. Note that some zones overlap in terms of their altitudinal/elevational ranges.

Eco-sedimentary zone	**Approximate altitude range (m OD)**	**Approximate SWLI range**	**Vegetation species assemblage**
Cowpen Marsh			
Sandy channel deposits	< -0.20*	< 38.00*	No vegetation.
Mudflat	-0.20 – 1.77	38.00 – 80.87	No vegetation.
Pioneer Marsh	1.77 – 2.00	80.87 – 85.87	30 % coverage of substrate. *Puccinellia maritima* with occasional *Salicornia europea*.
Low marsh	2.00 – 2.20	85.87 – 90.22	100 % coverage of substrate dominated by *Puccinellia maritima* and *Salicornia europea* with occasional *Aster tripoliu*, *Limonium vulgare*, *Sueda maritima*, *Spergularia* spp. and *Plantago maritima.*
Mid marsh	2.20 - 2.31	90.22 - 92.61	100 % of substrate characterised by an increase in the dominance of *Sueda maritima, Aster tripolium* and *Limonium vulgare* and a corresponding decrease in *Puccinellia maritima*. Increased species diversity at towards transition to high marsh, namely *Festuca rubra* and *Festuca ovina*.
High marsh	> 2.31^	> 92.61^	100 % coverage of substrate dominated by *Elymus pycnanthus* accompanied by *Festuca rubra*, *Festuca ovina*, and *Limonium vulgare.*
Roudsea Marsh			

Eco-sedimentary zone	Approximate altitude range (m OD)	Approximate SWLI range	Vegetation species assemblage
Sandflat	< 3.85*	< 91.07*	No vegetation.
Mudflat	3.85 – 4.00	91.07 – 92.87	No vegetation.
Pioneer Marsh	4.00 – 4.80	92.87 – 102.38	Increasingly vegetated with superficial pioneer salt marsh vegetation as altitude increases; *c*. 5 % vegetation coverage at 4.37 m OD (SWLI = 97.26) to approximately 95 % coverage at 4.61 m OD (SWLI = 100.12). Vegetation is predominantly composed of *Puccinellia maritima*, with increasing species diversity with altitude, incuding *Triglochin maritima*, *Cochlearia anglica*, *Atriplex littoralis* and *Plantago maritima*.
Low marsh	4.80 – 4.90	103.38 – 103.57	100 % coverage of substrate, dominated by *Puccinelia maritima and Triglochin maritima*, with *Aster maritima* and *Salicornia europea*. Isolated patches of *Juncus gerardii* and *Glaux maritima*.
Mid marsh	4.85 – 5.00	102.98– 104.76	100 % coverage of substrate, dominated by *Juncus maritima* with *Triglochin maritima, Cochlearia anglica* and *Spergularia maritima*.
High marsh	> 4.93^	> 103.93^	100 % coverage of substrate, dominated by *Phragmites* spp. and *Puccinelia maritima*, with *Atriplex prostrata*.
Thornham Marsh			
Sandy channel deposits	< 0.75*	< 56.25*	No vegetation.
Desiccated mudflat	1.44 – 2.44	67.03 – 82.66	< 1 % coverage; rare *Salicornea europea*.
Low marsh	2.44 – 2.76	67.03 – 91.41	*c*. 30 % coverage of substrate, dominated by *Salicornia europea* and *Spergularia maritima* with very rare *Limonium vulgare*.
Mid marsh	2.76 – 3.00	87.66 – 91.41	100 % coverage of substrate, dominated by *Puccinelia maritima* and

Eco-sedimentary zone	Approximate altitude range (m OD)	Approximate SWLI range	Vegetation species assemblage
			Halimione portulacoides with rare *Limonium vulgare*. Isolated patches of *Spergularia maritima* and *Plantago maritima*.
High marsh	> 3.00^	> 91.41^	100 % coverage of substrate, dominated by *Juncus maritimus*, *Halimione portulacoides*, with *Juncus gerardii*, *Plantago maritima* and *Limonium vulgare*.

* indicates altitude/SWLI value of lower boundary not recorded
^ indicates altitude/SWLI value of upper boundary not recorded

2. Field sampling locations

Figure 2 demonstrates the locations selected for description and sampling at each of the field sites. Table S2 provides a detailed description of the sediments at each of these locations. No samples were obtained from locations R03 - R06 inclusive for geotechnical testing because the contemporary surface sediments of interest were too thin (< 0.01 m) to allow oedometer compression testing. We did not obtain geotechnical samples from locations T02, T03 or T07, though we did collect disturbed samples for sedimentological analysis. Locations T02 and T03 were typical of the heavily desiccated areas of an unvegetated mudflat zone. These sediments were friable, which prohibited collection of undisturbed samples. Sediments at location T07 were similar in lithology to the main mid marsh zone at Thornham and only differed in terms of the vegetation species assemblage.

Field assessment and descriptions of sediment stiffness and moisture content are consistent with sediment type and eco-sedimentary zone at each of the sites. For example, sandy deposits were wet and loose; mudflat deposits ranged from damp to wet and very soft to soft; low marsh sediments were damp and soft to firm; and high marsh sediments were moist and very soft to soft. This suggests that the stiffest, most consolidated sediments are encountered in the low marsh. We noted the presence and increase in thickness (20 – 50 mm) with elevation of a mat of decomposing vegetation covering the main sediment horizon in the high marsh sediments (Table S2).

Table S2 General and detailed descriptions of sampling context and lithology at selected sampling locations.

Location ID	Altitude (m OD)	SWLI	Description	Lithology
Cowpen Marsh				
C01	-0.66	28.06	Sandy channel deposit. Occasional vertical bioturbation hollows (1 - 2 mm diameter).	Loose, wet, homogeneous, brown, slightly clayey, silty fine SAND.
C02	0.40	51.15	Mudflat. Located adjacent to incised tidal creek.	Very soft to soft, wet, homogeneous, brown and grey/black (at depths below 5 mm below ground level), slightly clayey, fine sandy SILT.
C03	1.36	72.02	Mudflat.	Very soft, moist, homogeneous, brown and grey/black (at depths below 5 mm below ground level), slightly fine sandy, clayey SILT.
C04	1.89	83.00	Hummocky pioneer marsh, some dead surface vegetation (*Salicornia europea* and *Puccinelia maritima*), some algal covering and some desiccation cracks. Rare vertical rootlets (< 1 mm diameter). Some coarser detritral organic matter present.	Soft, damp, heterogeneous brown, slightly organic, very slightly sandy, slightly clayey SILT.
C05	2.20	90.20	Low (*Puccinelia maritima)* marsh. A variable 0.05 – 0.30 m high cliff separates mudflat and pioneer marsh zones from the low marsh zone. Frequent rootlets (< 1 mm diameter) of vertical orientation.	Soft to firm, damp to moist, heterogeneous, brown, slightly clayey, spongy organic SILT.
C06	2.29	92.26	Mid marsh. Sample covered by 5 mm thick mat of dead vegetation. Organic matter consists of *in situ* roots (1 - 3 mm in diameter) and rootlets (< 1 mm diameter) and some decomposed organic matter.	Soft, damp, heterogeneous, brown, very slightly fine sandy, slightly clayey, spongy very organic SILT.
C07	2.52	97.24	High(*Elymus pycnanthus*) marsh. Sample covered by 20 - 30 mm thick mat of	Soft, damp, heterogeneous, dark brown, very slightly fine sandy, slightly clayey, spongy very organic SILT.

Location ID	Altitude (m OD)	SWLI	Description	Lithology
			undecomposed vegetation. Organic matter consists of in situ roots (1 - 3 mm in diameter) and rootlets (< 1 mm diameter) and some decomposed organic matter.	
C08	2.69	100.91	High (*Elymus pycnanthus*) marsh. Sample covered by 20 - 30 mm thick mat of undecomposed vegetation. Organic matter consists of *in situ* roots (1 - 3 mm in diameter) and rootlets (<1 mm diameter) and some decomposed organic matter.	Very soft, damp, heterogeneous, dark brown, very slightly fine sandy, slightly clayey, spongy very organic SILT.
Roudsea Marsh				
R01	3.83	90.81	Sandflat. Frequent vertical bioturbation hollows (1 - 2 mm diameter).	Loose, moist, homogeneous, light brown/beige, very slightly clayey, very silty, fine SAND.
R02	4.00	92.87	Mudflat (< 5 % total vegetation coverage).	Soft, moist, thinly laminated, brown (surface) and grey/black (at depths below 5 mm below ground level), clayey, fine sandy SILT.
R03	4.37	97.25	Mudflat (< 5 % total vegetation coverage). Desiccation cracked and friable/flaky. Thin layer (< 1 cm) overlying sand.	Soft, moist, thinly laminated, brown (surface) and grey/black (at depths below 5 mm below ground level), clayey, fine sandy SILT.
R04	4.87	103.15	Mudflat/pioneer marsh. Increased vegetation covering (40 – 50 %). Thin layer (< 1 cm) overlying sand. Largely modified (humified) sand layer.	Soft, moist, thinly laminated, brown (surface) and grey/black (at depths below 5 mm below ground level), clayey, fine sandy SILT.
R05	4.70	101.19	Mudflat/pioneer marsh (40 – 50 % vegetation coverage). Thin layer (< 1 cm) overlying sand. Largely modified (humified) sand layer.	Soft, moist, thinly laminated, brown (surface) and grey/black (at depths below 5 mm below ground level), clayey, fine sandy SILT.
R06	4.61	100.11	Mudflat/pioneer marsh (95 % vegetation coverage). Increased vegetation covering and	Soft, damp, heterogeneous, light brown with orange mottling, slightly organic, clayey, fine sandy SILT.

Location ID	Altitude (m OD)	SWLI	Description	Lithology
			greater species diversity. Thin layer (< 1 cm) overlying sand. Largely modified (humified) sand layer.	
R07	4.82	102.60	Low (*Puccinelia maritima*) marsh. Frequent rootlets (< 1 mm diameter) with random orientation.	Soft to firm, moist, light brown, very slightly clayey, slightly organic, fine sandy SILT.
R08	4.96	104.25	Hummocky mid (*Juncus maritimus)* marsh. Frequent rootlets (< 1 mm diameter) with random orientation.	Firm, moist, heterogeneous, brown with orange mottling, slightly organic, slightly clayey, fine sandy SILT.
R09	4.89	103.43	Low (*Puccinelia maritima*) marsh in topographic low at rear of marsh. Frequent rootlets (< 1 mm diameter) with random orientation.	Soft to firm, moist, light brown with orange mottling, slightly fine sandy, organic, clayey SILT.
R10	5.12	106.19	High (*Phragmites* spp.) marsh. Frequent rootlets (< 1 mm diameter) with random orientation.	Very soft, moist, heterogeneous, brown with orange mottling, very slightly fine sandy, clayey, organic SILT.
Thornham Marsh				
T01	0.41	50.89	Sandy channel deposit. Occasional vertical bioturbation hollows (1 - 2 mm diameter) and detrital sea weed covering.	Very loose, wet, homogeneous, light brown/beige, medium SAND.
T02	1.69	70.92	Heavily desiccated and cracked mud.Frequent vertical bioturbation hollows (1 - 2 mm diameter) and occasional vertical rootlets (< 0.5 mm diameter).	Very soft to soft, moist to damp, thinly laminated, brown (oxidised/surface), black (sub-surface) and orange/red (burrows), clayey, very fine sandy SILT.
T03	1.99	75.63	Heavily desiccated and cracked mud.Frequent vertical bioturbation hollows (1 - 2 mm diameter) and occasional vertical rootlets (<	Very soft to soft, moist, heterogeneous, mottled red/orange, organic, slightly clayey SILT.

Location ID	Altitude (m OD)	SWLI	Description	Lithology
			0.5 mm diameter).	
T04	1.50	67.89	Soft mud within tidal creek. Frequent vertical bioturbation hollows (1 - 2 mm diameter).	Very soft, damp homogeneous, brown (surface), black (at depths > 5 cm bgl) and orange/red (walls of bioturbation hollows), very slightly clayey, very fine sandy SILT.
T05	2.51	83.80	Low (*Salicornia europea*) marsh. Some desiccation cracking on surface. Frequent vertical bioturbation hollows (1 - 2 mm diameter) and frequent vertical rootlets (< 0.5 mm diameter).	Very soft to soft, moist, heterogeneous, brown with orange mottling, slightly organic, very slightly clayey, very fine sandy SILT.
T06	2.98	91.03	Mid (*Limonium vulgare*) marsh. Some salt pans and pools and minor, shallow creeks. Frequent rootlets (< 1 mm diameter) with random orientation.	Very soft to soft, moist, heterogeneous, brown with orange mottling, organic, very slightly clayey, very fine sandy SILT.
T07	2.94	90.52	Creek-fringing marsh assemblage. Occasional rootlets (< 1 mm diameter) with random orientation.	Soft, moist, heterogeneous, brown, organic, clayey SILT.
T08	3.03	91.80	High (*Halimione portucaloides*) marsh. Uppermost 50 mm consists largely of decaying biomass.	Firm, dry to moist, heterogeneous, brown with orange mottling, organic, very clayey SILT.
T09	3.14	93.55	High (*Halimione portucaloides*) marsh with greater vascular plant species diversity than location T08. Uppermost 50 mm consists largely of decaying biomass.	Soft, moist to damp, heterogeneous, brown, organic SILT.

3. Monte Carlo Analysis

3.1 Determining number of model simulations

To ensure an adequate number of simulations to fully capture the accuracy and precision of estimates of post-depositional lowering (PDL, m) within each synthetic core, we ran 5000 simulations and calculated the mean and standard deviation (i.e. the key model outputs) of PDL for each depth within the synthetic core. We then selected random sub-samples of increasing number (from n = 1 to n = 5000) from the population of 5000 simulations. For each sub-sample, we calculated the mean and standard deviation of PDL at each depth in the core. We used linear regression to compare the model predictions for each sub-sample with those from the full population, quantifying their performance using r^2 values. Figure S2 shows model performance (r^2) for each sub-sample against the number of simulations in that sub-sample. This demonstrates that variability in model outputs is effectively absent when the number of simulations exceeds 400 (i.e. any 400 simulations should give the same predicted means and standard deviations). Hence, model predictions for each stratigraphic succession are based on 1000 iterations – at least twice the minimum required number of iterations.

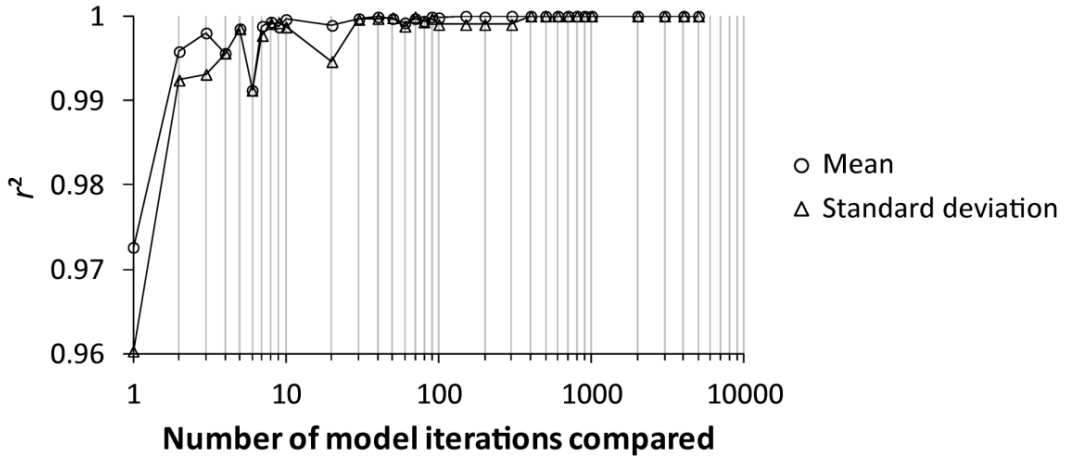

Figure S2 Comparison of model performance (y-axis) against number of simulations (x-axis). Performance is quantified using r^2 for the relationship between predicted means and standard deviations of PDL from a sub-sample of simulations and those from the full population.

3.2 Regression model error

Model uncertainty results from regression model errors. Where appropriate, we used the standard error of the estimate as regression model error. However, where the form of the residuals deviated from a normal distribution (i.e. if the residuals failed a Shapiro-Wilk normality test), we used a uniformly distributed error term (± half the range of the modelled residuals). Regression model error terms are summarised in Table S3.

All other parameters used in the modelling procedure were treated deterministically (initial palaeo marsh surface elevation, depth in core, layer thickness, gravitational acceleration). Subsequently calculated parameters relating to, for example, stress distribution are derived from both deterministic and stochastic parameters, allowing uncertainty in input/calculated parameters to be propagated through the model into predicted PDL. The resultant PDL distributions are characterised using their mean and standard deviation.

Table S3 Summary of error terms for regression models used in the generation of synthetic stratigraphic successions.

Predicted (predictor) variable	**Residuals passed Shapiro-Wilk normality test?**	**Regression model error distribution**	**± error term**
Specific gravity (loss on ignition)	No	Uniform	0.108
e_1 (loss on ignition)	No	Uniform	1.220
C_r (loss on ignition)	No	Uniform	0.125
C_c (loss on ignition)	Yes	Normal	0.276
Yield stress, kPa (SWLI)	Yes	Normal	2.734

References

Admiralty Tide Tables, 2005. Hydrographer of the Navy, Taunton, Somerset.

Allen, J.R.L., 2000. Morphodynamics of Holocene salt marshes: A review sketch from the Atlantic and Southern North Sea coasts of Europe. Quaternary Science Reviews, 19(12), 1155-1231.

Carniello, L., D'Alpaos, A. and Defina, A., 2011. Modeling wind waves and tidal flows in shallow micro-tidal basins. Estuarine, Coastal and Shelf Science, 92, 263 – 276.

Gray, A.J., 1972. The Ecology of Morecambe Bay. V. The Salt Marshes of Morecambe Bay. Journal of Applied Ecology, 9, 207 – 220.